https://doi.org/10.5194/egusphere-2026-2729
Preprint. Discussion started: 27 May 2026

Tidal modulation of nitrate supply and chlorophyll-a in the Amazon shelf–offshore continuum

Amine M'hamdi[1, 2, 3], Ariane Koch-Larrouy[1,2], Isabelle Dadou[2], Carina Regina de Macedo[2,4,7], Fernand Assene[2,5,6], Vincent Vantrepotte[7], Guillaume Morvan[2], Alex Costa da Silva[3]

[1]CECI CNRS/Cerfacs/IRD, Université de Toulouse, Toulouse, France.
[2]LEGOS, Université de Toulouse, CNRS, OMP, IRD, Toulouse, France.
[3]Departamento de Oceanografia, Universidade Federal de Pernambuco (DOCEAN/UFPE), Recife, Brazil.
[4]Earth Observation and Geoinformatics Division, National Institute for Space Research (INPE), São José dos Campos, Brazil.
[5]Mercator Ocean International, 31400 Toulouse, France.
[6]Department of Maritime Navigation and Information Systems, National Advanced School of Maritime and Ocean Science and Technology (NASMOST), University of Ebolowa, P.O. Box: 292 Kribi, Cameroon.
[7]Univ. Littoral Côte d'Opale, CNRS, Univ. Lille, IRD, UMR 8187- LOG- Laboratoire d'Océanologie et de Géosciences, F-62930 Wimereux, France.

Correspondence to: Amine M'hamdi (abn.mhamdi@email.com)

Abstract. The Amazon shelf–offshore continuum is a dynamic biogeochemical hotspot of the tropical Atlantic, where river discharge, ocean circulation, and strong tides interact to shape nutrient and phytoplankton distributions. The Amazon plume and regional circulation have been widely studied and are known to strongly influence nutrient availability and biological productivity in this region. However, shelf-break tides remain an overlooked pathway linking physical energy to offshore fertilization, and their contribution to seasonal and intraseasonal biogeochemical variability remains unclear. Here, we quantify how tidal dynamics, including internal tides, modulate nitrate supply and chlorophyll distributions from the Amazon shelf to offshore waters. We use a high-resolution coupled physical–biogeochemical model (1/36°), evaluated against climatological, satellite, and in situ observations. The model reproduces the main observed patterns of surface nitrate and chlorophyll, as well as key vertical features such as the nitracline and the deep chlorophyll maximum. We show that tides strongly enhance upward nitrate transport, increasing surface nitrate by more than 50% over the northern shelf, along the shelf break, and within the main internal-tide pathway. This tidally supplied nitrate fuels offshore phytoplankton growth, increasing chlorophyll by about 15–50%, while reducing surface chlorophyll near the Amazon mouth by 30–40%.Seasonally, surface chlorophyll and nitrate are higher over the Amazon shelf during April–June but lower offshore, revealing a marked cross-shelf contrast. When the tidal contribution is isolated, a similar but weaker spatial structure emerges, with a cone-shaped chlorophyll anomaly extending from the shelf break toward the offshore internal-tide propagation region. Remarkably, tides account for about 63% of the total seasonal variability in surface nitrate, meaning that tidal forcing alone explains more than half of the seasonal nutrient signal. At intraseasonal timescales, tides generate a clear spring–neap rhythm of about 15 days in both nitrate and chlorophyll. This spring–neap tidal pulse propagates from the shelf break toward offshore waters and is especially pronounced near the deep chlorophyll maximum, where oscillations of the

https://doi.org/10.5194/egusphere-2026-2729
Preprint. Discussion started: 27 May 2026

upper nitracline periodically modulate nitrate availability and drive a corresponding chlorophyll response., where chlorophyll variability is nearly doubled when tides are included. The concurrent increase in nitrate variability indicates that this spring–neap phytoplankton response is sustained by tidally driven nutrient supply.

These findings identify internal tides as a key biogeochemical driver of the Amazon shelf–offshore continuum, linking tidal energy to nutrient injection, offshore fertilization, seasonal redistribution, and rhythmic ecosystem variability in the western tropical Atlantic.

1. Introduction

The headings Physical processes regulate upper-ocean biogeochemistry by controlling stratification, tracer transport, and the rate at which nutrients are supplied to the euphotic layer. In particular, at the shelf break, barotropic tidal currents interacting with the steep 200–2000 m continental slope in a stratified ocean generate energetic internal tides. These tides radiate offshore and dissipate away from their generation sites, promoting diapycnal mixing and vertical exchanges across density surfaces (Baines, 1982; Egbert and Ray, 2000; Munk and Wunsch, 1998). Such processes can substantially modify nitrate supply, chlorophyll distributions, and primary production; however, their cumulative impacts remain difficult to quantify because the relevant physical–biogeochemical couplings are multiscale and often under-resolved in coupled ocean physical–biogeochemical models (Capuano et al., 2025; Jacobsen et al., 2023; Ma et al., 2023; Mahadevan, 2016; M'hamdi et al., 2025). This limitation is especially acute in regions where several energetic processes interact across different spatio-temporal scales. In the western tropical Atlantic ocean, even recent regional coupled physical-biogeochemical models that include key processes such as N_2 fixation still struggle to reproduce important features of the Amazon-plume system, notably the offshore extension of productive waters, suggesting that major mechanisms remain missing or insufficiently represented (Gévaudan et al., 2025; Louchard et al., 2021).

The Amazon shelf–offshore continuum (Figure 1) is an exceptional natural laboratory for such coupling. There, freshwater forcing, tides, western boundary circulation, mesoscale variability, and strong upper-ocean stratification interact from the shelf to the open ocean, while the shelf break itself represents a recognized hotspot of internal-tide generation embedded within a region of strong seasonal circulation variability (Assene et al., 2024; Ruault et al., 2020; Tchilibou et al., 2022). The regional circulation (Figure 1) is dominated by the North Brazil Current (NBC), its retroflection toward the North Equatorial Countercurrent (NECC), and the associated mesoscale eddy field(Aguedjou et al., 2019; Didden and Schott, 1993; Fratantoni and Glickson, 2002; Richardson et al., 1994; Silva et al., 2009). This circulation exhibits a marked seasonal cycle: during April–May–June (AMJ), the NBC is weaker and more coastally trapped, mesoscale activity is reduced, and Amazon discharge is higher, whereas during August–September–October (ASO), the NBC becomes broader, deeper, and stronger, and eddy kinetic energy increases (Aguedjou et al., 2019; Johns et al., 1998, p.19; Molleri et al., 2010). These seasonal changes strongly influence upper-ocean density structure and pycnocline properties, with important consequences for internal tides dynamics (Barbot et al., 2021; Ruault et al., 2020; Silva et al., 2005, p.200; Tchilibou et al., 2022).

Regional biogeochemistry is also strongly shaped by the Amazon River plume. As the largest freshwater source to the global ocean, the Amazon discharges on average about 177 493 m^3s-1 and influences a vast portion of the western tropical Atlantic ocean, with a pronounced seasonal cycle peaking in late spring to early summer (HYBAM, 2018; Louchard et al., 2021; Olivier et al., 2024). After leaving the shelf, plume waters are entrained by the NBC and may spread northwestward toward the Caribbean or eastward depending on the state of the NBC, its retroflection, and associated rings (Fratantoni and Glickson, 2002; Johns et al., 1998; Olivier et al., 2024; Subirade et al., 2023). Biogeochemically, the plume sustains large phytoplankton blooms, but its chlorophyll response remains spatially heterogeneous because light availability, turbidity, terrestrial dissolved organic matter, and nutrient consumption evolve along the aging plume (Gévaudan et al., 2025; Lefèvre et al., 2017; Muller-Karger et al., 1988; Müller-Karger et al., 1989; Olivier et al., 2022; Smith Jr and Demaster, 1996; Subramaniam et al., 2008). Near the Amazon mouth, phytoplankton growth is mainly limited by light, whereas farther offshore nitrogen commonly becomes the dominant limiting nutrient, making vertical nitrate supply and nitracline depth key controls on upper-ocean chlorophyll distribution(Demaster and Pope, 1996; Gévaudan et al., 2025; Goes et al., 2014).

Against this background, tidal forcing appears to be a prominent but still incompletely resolved control on regional biogeochemical variability (Ruault et al., 2020). Over the shelf, barotropic tides enhance bottom friction and vertical mixing, can resuspend sediments, modify light availability, and may also influence plume pathways (Hu et al., 2008; Kossack et al., 2023; Sharples et al., 2007; Xing et al., 2021). At the shelf break, barotropic tidal currents interacting with the sharp 200–2000 m slope in a stratified ocean generate energetic internal tides that radiate offshore and dissipate away from their generation sites, producing diapycnal mixing and vertical exchanges across density surfaces (Baines, 1982; Egbert and Ray, 2000; Munk and Wunsch, 1998). Along the Brazilian Equatorial Margin, six main internal-tide generation sites, commonly labeled A to F, have been identified, with the strongest generation at site A (Figure 1) (Assene et al., 2024; Magalhaes et al., 2016; Tchilibou et al., 2022). The resulting low-mode internal tides can propagate horizontally over more than 100–200 km and enhance mixing both near their generation sites and along their propagation pathways(Assene et al., 2024; Barbot et al., 2021; De Macedo et al., 2023; Goret et al., 2025; Kouogang et al., 2025a; Tchilibou et al., 2022). Tidal forcing may therefore affect nitrate and chlorophyll concentrations through the combined action of its barotropic and baroclinic components, but this coupling remains poorly quantified at regional scale.

Tidal impacts on nitrate and chlorophyll are, however, not mechanically unique. A first mechanism is primarily redistributive: internal tides vertically displace isopycnals and the deep chlorophyll maximum (DCM), thereby modifying the light environment experienced by phytoplankton and altering the apparent upper-ocean chlorophyll signal (De Macedo et al., 2026; Gaxiola-Castro et al., 2002; Kim et al., 2018; M’hamdi et al., 2025; Muacho et al., 2014). A second mechanism is tidal mixing, which can homogenize the chlorophyll profile and enhance nitrate fluxes toward the nitracline and the productive layer, thereby stimulating new production in areas where nutrient limitation prevails. (Jacobsen et al., 2023; Kossack et al., 2023; M’hamdi et al., 2025; Sharples et al., 2007; Tuerena et al., 2019). Recent observations collected during the AMAZOMIX campaign support the coexistence of both effects off the Amazon shelf, with internal tides modulating the depth of the chlorophyll maximum and episodic mixing events associated with enhanced chlorophyll concentrations in the upper water column (M'hamdi et al., 2025). At the same time, recent work on the Amazon plume has emphasized that chlorophyll variability in this region cannot be interpreted from nutrient supply alone, because light attenuation and the remineralization of terrestrial dissolved organic matter also exert strong controls on plume productivity and offshore extension (Gévaudan et al., 2025). Despite this growing evidence, the regional expression of tidal effects on nitrate and chlorophyll concentrations over the Amazon shelf and adjacent offshore waters remains poorly constrained.

The efficiency of this tidal-biogeochemical coupling is also expected to vary in time because the regional background state changes markedly over the year. During AMJ, the Amazon discharge is high, the pycnocline is shallower and slightly stronger, and both the NBC and mesoscale eddy activity are relatively weak. During ASO, river discharge decreases, the pycnocline deepens, and both the NBC and mesoscale variability intensify (Aguedjou et al., 2019; Barbot et al., 2021; Tchilibou et al., 2022). These changes affect not only plume structure and stratification, but also the generation, propagation, and dissipation of internal tides. In particular, stronger conversion and local dissipation of internal-tide energy have been reported in AMJ than in ASO, whereas the stronger background circulation in ASO favors a larger contribution of incoherent internal tides (Barbot et al., 2021; Tchilibou et al., 2022). In addition to their influence on the seasonal mean state, tides may also imprint submonthly variability through the spring-neap cycle. The nonlinear interaction between the dominant semidiurnal constituents M2 and S2 produces a fortnightly modulation at the MSf period of 14.77 days (Ray and Susanto, 2016). In several energetic marine environments, this spring-neap modulation has been linked to variations in sea surface temperature, suspended matter, nutrient supply, and chlorophyll, either through bottom-driven mixing or through changes in internal-wave activity(Capuano et al., 2025; De Macedo et al., 2026; Ray and Susanto, 2016; Sharples et al., 2007; Xing et al., 2021; Zaron et al., 2023).

What remains unresolved is therefore not whether tides matter, but how barotropic and baroclinic tides jointly shape the interaction between nitrate supply and chlorophyll variability in a system already structured by river discharge, circulation, and plume biogeochemistry. This gap is also methodological: high-resolution regional twin simulations with and without tides remain extremely rare, even though such configurations are among the most direct ways to isolate the net tidal contribution from the strong background variability. More broadly, constraining the regional biogeochemistry of the Amazon-plume system remains a major scientific challenge, because key processes are still incompletely represented in existing models (Gévaudan et al., 2025; Louchard et al., 2021). Here, we address three main scientific questions: how do tides modify the mean surface and subsurface distributions of nitrate and chlorophyll in the internal tides pathway; how does that response differ between the contrasted AMJ and ASO seasons; and do tides imprint a detectable MSf spring-neap signature in the modeled nitrate and chlorophyll fields? To answer these questions, we use a high-resolution 1/36° coupled NEMO-PISCES configuration and twin simulations performed over 2013–2016 with and without tides, with the aim of quantifying the regional tidal contribution and providing a process-based framework for interpreting observed nitrate and chlorophyll variability off the Amazon shelf.

https://doi.org/10.5194/egusphere-2026-2729
Preprint. Discussion started: 27 May 2026

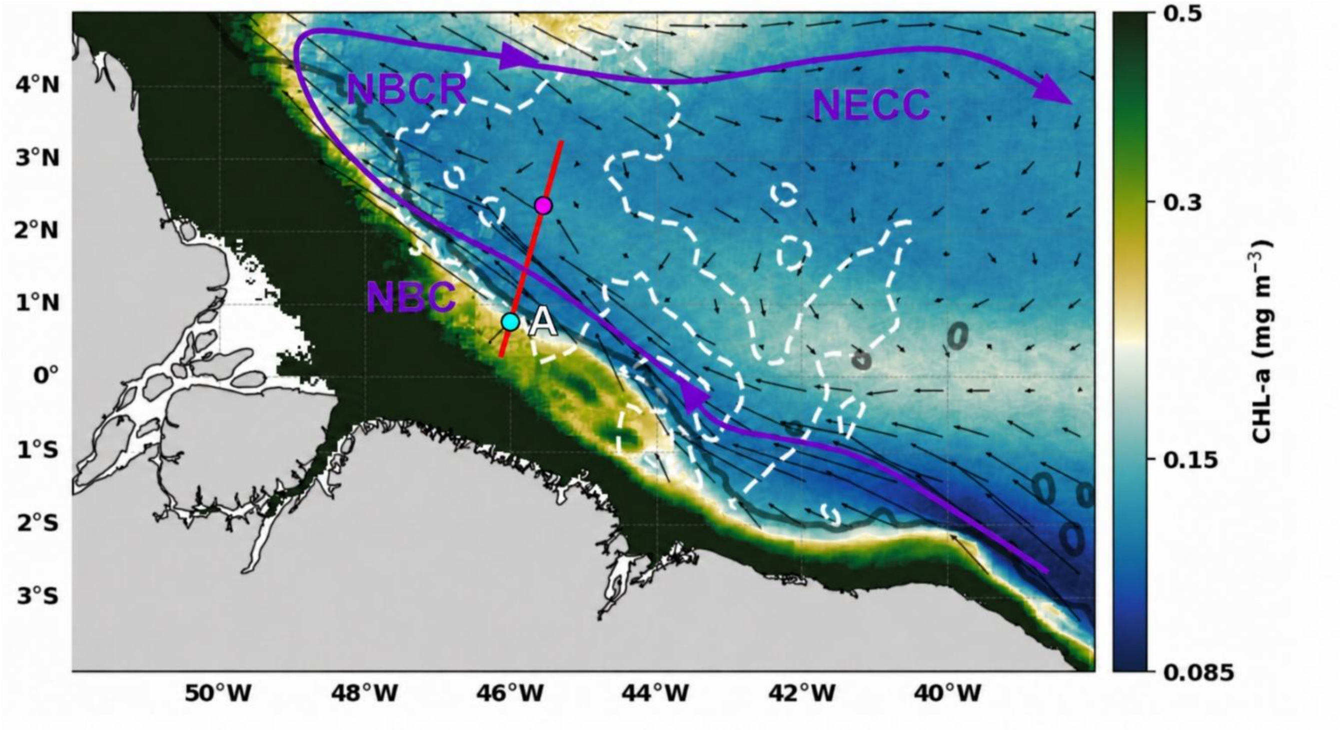

Figure 1 : Mean surface chlorophyll-a concentration (log$_{10}$ scale) over the Amazon shelf–offshore continuum for the 2013–2016 period, derived from CCI ocean-color products. The dashed white contour indicates the 1.8 m M2 internal tide amplitude from MIOST. Black arrows denote the mean surface geostrophic currents from DUACS, while purple arrows highlight the dominant regional current system. The red line marks the main internal tide (IT) propagation path named here transect A, and cyan symbols indicate the primary IT generation site and the magenta one the main dissipation site. The semi-transparent black line delineates the continental shelf break.

2. Data and Methods

2.1 Model configuration and numerical experiments

A high-resolution coupled physical–biogeochemical regional configuration, hereafter referred to as AMAZON36-BIO, was developed to investigate fine-scale physical and biogeochemical processes over the Amazon shelf and the adjacent western tropical Atlantic Ocean. The model domain extends from 54.7°W to 35.3°W and from 5.5°S to 6°N, with a horizontal resolution of 1/36° corresponding to approximately 3 km.

The physical configuration, named AMAZON36, is based on the NEMO ocean circulation model and was designed to explicitly resolve the main internal-tide generation sites along the Brazilian Equatorial Margin, as well as their offshore propagation pathways. Earlier regional configurations used in this area were either too coarse to adequately represent these processes or too limited in spatial extent to include the main generation sites and offshore propagation regions. By

https://doi.org/10.5194/egusphere-2026-2729
Preprint. Discussion started: 27 May 2026

combining high horizontal resolution with a sufficiently large domain, AMAZON36 is able to resolve low-mode internal tides over the western tropical Atlantic Ocean. The study is based on a set of twin simulations performed with and without tidal forcing, following the experimental design of Assene et al. (2024). The simulation including tidal forcing is hereafter referred to as TIDES, whereas the simulation without tidal forcing is referred to as NOTIDES. The net tidal contribution to any variable is defined as:

$$\Delta = \mathrm{TIDES} - \mathrm{NOTIDES}$$

The AMAZON36 physical configuration was coupled to the PISCES v4.0 biogeochemical model, yielding the AMAZON36-BIO setup. This coupled configuration was specifically designed to investigate the effects of tides on biogeochemical properties, with a particular focus on nitrate and chlorophyll concentrations. Biogeochemical initial and open-boundary conditions for PISCES were prescribed from the Copernicus Marine Service global biogeochemical hindcast product GLOBAL_MULTIYEAR_BGC_001_029, distributed by Mercator Ocean International. This product has a horizontal resolution of 1/4°, 75 vertical levels, and daily temporal frequency over the 1993–2022 period. The biogeochemical variables used include dissolved oxygen, nitrate, phosphate, silicate, dissolved iron, chlorophyll, phytoplankton carbon biomass, primary production, pH, and surface partial pressure of CO_2.
Riverine biogeochemical inputs were prescribed from the climatological product BIOMERGLORYS2V3_river.orca025deg, provided by Mercator Ocean International. This dataset supplies dissolved inorganic and organic forms of nitrogen, phosphorus, silicon, and carbon, allowing the biogeochemical influence of river discharge to be represented. The vertical grid comprises 75 z-levels, with enhanced resolution near the surface, including 23 levels in the upper 100 m and 8 levels in the upper 10 m. Layer thickness increases progressively with depth and reaches approximately 160 m near the bottom. This vertical discretization is appropriate for resolving upper-ocean stratification, pycnocline variability, and low-mode internal-tide dynamics. Atmospheric forcing is provided by the ERA5 reanalysis. Amazon River discharge is prescribed from monthly discharge fields simulated by ISBA-CTRIP. These discharge fields are adjusted using a uniform multiplicative factor of 0.9, determined from comparison with the interannual HYBAM discharge time series. The simulations include a 3-year spin-up period from 2010 to 2012, followed by a 4-year analysis period from January 2013 to December 2016. Monthly and daily outputs are used depending on the diagnostic considered. In PISCES, chlorophyll-a is represented separately for two phytoplankton functional groups, nanophytoplankton and diatoms. In this study, total chlorophyll concentration is computed as the sum of chlorophyll associated with these two groups.

2.2 Observational dataset

2.2.1 Surface nitrate concentration

The simulated surface nitrate concentration was compared with the CARS (CSIRO Atlas of Regional Seas) climatology (Ridgway et al., 2002). Since the model and observational products are defined on different grids, the model fields were interpolated onto the observational grid using a linear interpolation.

2.2.2 Surface chlorophyll-a concentrations

For surface chlorophyll-a, we used the daily Ocean Colour CCI L3 product (https://doi.org/10.48670/moi-00282) distributed by the Copernicus Marine Service and implemented by Mercator Ocean International. This multisensor product is based on ESA Climate Change Initiative (ESA-CCI) observations and combines measurements from SeaWiFS, MODIS, MERIS, VIIRS-SNPP, and OLCI onboard Sentinel-3A and Sentinel-3B. It provides daily global chlorophyll-a fields at 4 km spatial resolution.

2.2.3 Altimetric internal-tide signatures: MIOST-IT and baroclinic flux

To characterize the spatial distribution of coherent internal-tide surface signatures and to support the interpretation of the model results, we used the MIOST-IT products, *Multivariate Inversion of Ocean Surface Topography – Internal Tide*, distributed by AVISO+ (doi: 10.24400/527896/a01-2022.003). MIOST-IT provides climatological estimates of internal-tide sea surface height signatures derived from a simultaneous inversion of mesoscale and internal-tide contributions using the global multi-mission altimetry record. In its current release, MIOST-IT provides amplitude and phase estimates for four tidal constituents, M2, S2, K1, and O1, for both mode-1 and mode-2 internal tides. These estimates are based on all available altimetry missions between January 1993 and June 2017 and are distributed on a regular 1/10° × 1/10° grid. In this study, the climatological M2 internal-tide amplitude was used to identify the main generation sites and preferential offshore propagation pathways over the Brazilian Equatorial Margin. It was also used to define specific analysis subdomains and to provide an observational reference for interpreting the modeled physical and biogeochemical variability.

To further document internal-tide propagation in the model, we computed model-derived energetic diagnostics following the framework of Kelly et al. (2010). In particular, we estimated the depth-integrated baroclinic energy flux. Only the M2 harmonic was considered, as it is the dominant tidal constituent in the study region and accounts for approximately 70% of the tidal energy (Beardsley et al., 1995; Gabioux et al., 2005; Prestes et al., 2018; Fassoni-Andrade et al., 2023).

The depth-integrated baroclinic energy flux is defined as:

The depth-integrated baroclinic energy fluxes is defined as :

$$\mathbf{F}_{\mathbf{bc}} = < \int_{-H}^{\eta} U_{bc} P_{bc} dz >$$

where U denotes velocity, P pressure, η sea-surface elevation, and z the vertical coordinate. The baroclinic energy flux Fbc therefore describes both the direction and magnitude of internal-tide energy propagation through the water column.

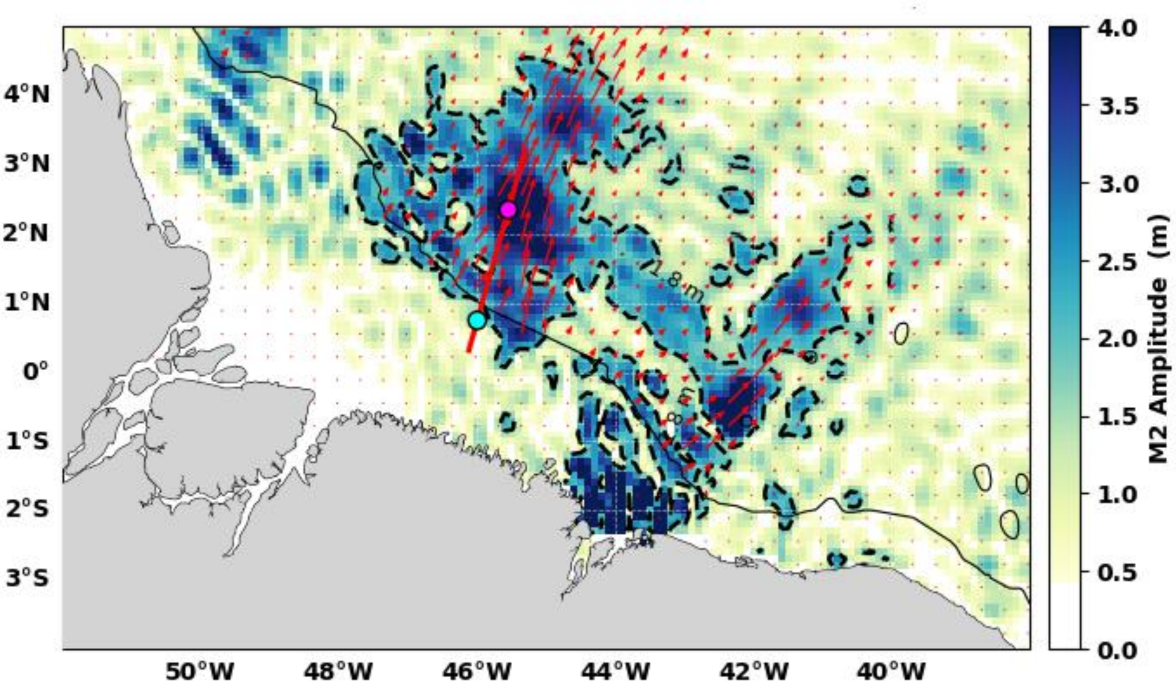

Figure 2: Amplitude of the M2 component of internal tides (MIOST-IT product) and The model depth-integrated baroclinic energy flux (red arrow) for M2. Black line is the 1000m isobath and the black dashed contour is the 1.8 contour for M2 amplitude.

2.2.4. Surface geostrophic currents

The surface geostrophic currents were obtained from the delayed-time DUACS altimetry product over 2013–2016(https://doi.org/10.48670/moi-00149). The zonal and meridional components of absolute geostrophic velocity were used to characterize the large-scale surface circulation in the study region.

2.2.5 *In situ* observations from the AMAZOMIX campaign

Model outputs (2013-22016) were also compared with in situ observations collected during the AMAZOMIX campaign(08/2021 to 10/2021). Because in situ biogeochemical observations are scarce in the Amazon shelf–offshore region and no comparable measurements are available for the simulated period, this comparison was used as a qualitative assessment of the model's ability to reproduce the observed cross-shelf gradients and vertical tracer structuresin the August to October period. The comparison was based on 32 hydrographic stations sampled (Figure 4). For each station, the model profile was extracted at the closest model grid point for the corresponding sampling season.

The closest grid point to each station was identified using a k-dimensional tree algorithm implemented with scipy.spatial.cKDTree and built from the model horizontal grid. This nearest-neighbor approach preserves the native model

https://doi.org/10.5194/egusphere-2026-2729
Preprint. Discussion started: 27 May 2026

grid while allowing direct station-based profile extraction. The extracted model profiles were then analyzed together with the observations, with particular focus on nitrate and chlorophyll-a concentrations in the upper 125–200 m.

2.2.6 Eddy Kinetic Energy data

Surface eddy kinetic energy (EKE) was derived from the SSALTO/DUACS multi-mission altimetry monthly climatology product distributed by AVISO+ (doi: 10.24400/527896/AVISO-2026.002). This product provides Level-4 gridded fields on a regular 0.25° × 0.25° global grid, with monthly temporal resolution. EKE is computed from the zonal and meridional geostrophic velocity anomalies derived from the gridded sea level anomaly (SLA) field of the CMEMS SEALEVEL_GLO_PHY_L4_REP_OBSERVATIONS_008_047 product, based on the DUACS DT2018 reprocessing:

$$\mathrm{EKE} = \frac{u'^2 + v'^2}{2}$$

where u' and v' are the zonal and meridional geostrophic velocity anomalies, respectively. EKE is expressed in $\mathrm{cm^2\ s^{-2}}$. Monthly fields are obtained by averaging all daily SLA-derived EKE fields available within each month, with the nominal date set to the 15th day of the month.

For this study, monthly EKE fields were extracted over the Brazilian Equatorial Margin, from 52°W to 38°W and from 4°S to 5°N, for the period 1993–2020. Seasonal climatologies were then computed by averaging the corresponding monthly fields for January–March, April–June, July–September, and October–December. A light Gaussian smoothing with $\sigma = 1.2$ grid points was applied to reduce small-scale noise, and the resulting fields were masked outside the model domain to ensure consistency with the other satellite and model products used in this study. Finally, region-averaged EKE values were computed using latitude-cosine area weighting.

2.3 Statistical evaluation of model performance

The model–data comparison was quantified using complementary statistical metrics that characterize different aspects of model skill. These include the mean bias, mean absolute error (MAE), median absolute error (MedAE), root mean square error (RMSE), centered RMSE when applicable, the Pearson spatial correlation coefficient rrr, and the standard deviation ratio between model and observations.

These metrics were selected because they provide complementary information on model performance. Bias measures systematic over- or underestimation. MAE and MedAE quantify the typical magnitude of the error and are less sensitive than RMSE to isolated extreme values. RMSE emphasizes larger mismatches and is therefore useful for identifying whether the comparison is influenced by localized strong discrepancies. The correlation coefficient evaluates the degree to which the model reproduces the observed spatial organization, independently of absolute amplitude. Finally, the standard deviation ratio provides information on whether the model overestimates or underestimates the spatial variability of the observed fields. Taken together, these metrics allow a more robust and interpretable assessment of model skill than any single metric alone.

2.4. Wavelet-based analysis of submonthly variability and spring–neap tidal modulation

2.4.1 Submonthly variability and detection of the spring–neap signal

To determine whether tides imprint a submonthly signal on biogeochemical tracers, we analyzed daily outputs from the TIDES and NOTIDES simulations over 2013–2016. Time series of nitrate and chlorophyll-a were extracted at selected fixed locations and along the cross-shelf transect.

The spring–neap modulation was investigated at the MSf period (14.77 days), which results from the nonlinear interaction between the dominant semidiurnal tidal constituents. Before spectral analysis, each time series was linearly detrended and normalized by its standard deviation.

2.4.2 Wavelet analysis and Global Wavelet Spectrum

A continuous Morlet wavelet transform was applied to the daily time series using the PyCWT package, following Torrence and Compo, 1998. Wavelet analysis is particularly well suited to oceanographic and ecological time series because it resolves variance simultaneously in time and frequency, making it appropriate for non-stationary signals. In this study, it was used to identify and quantify the time-varying spectral energy associated with the fortnightly tidal band.

For each time series, the Global Wavelet Spectrum (GWS) was computed as the time-averaged wavelet power spectrum. The GWS provides the total variance distribution as a function of period and was used to compare the spectral content of the TIDES, NOTIDES, and, where available, satellite chlorophyll time series. This approach follows recent applications where wavelet analysis has proven effective in extracting tidal signatures in chlorophyll-a variability (De Macedo et al., 2026).

To assess the statistical significance of spectral peaks, GWS was compared against a red-noise background spectrum modeled as a first-order autoregressive process [AR(1)], and the 95% confidence level was used as the significance threshold.

3. Model Evaluation

3.1 Nitrate Mean Surface Spatial Pattern

The annual mean surface nitrate concentrations averaged over 2013–2016 are shown for the NOTIDES simulation, together with the model–data differences relative to the CARS climatology (Figure 3). Overall, the model reproduces the main large-scale spatial patterns of surface nitrate, including the enhanced concentrations associated with the Amazon River plume. This agreement indicates that the model captures the first-order influence of riverine nutrient inputs on surface biogeochemical conditions in the western tropical Atlantic.

Regional discrepancies are nevertheless evident. In particular, the model shows positive nitrate biases in the equatorial region, consistent with the known tendency of coupled physical–biogeochemical models to overestimate nutrient concentrations and associated primary production in equatorial environments (Gévaudan et al., 2025; Louchard et al., 2021).

Despite these biases, simulated nitrate concentrations remain within the correct order of magnitude in plume-influenced waters, supporting the model's ability to represent the broad nitrate distribution over the Amazon shelf–offshore continuum. The comparison with CARS should, however, be interpreted with caution. CARS is an interpolated climatology provided at a relatively coarse horizontal resolution of 1/2°, and may therefore smooth sharp gradients and small-scale structures resolved by the 1/36° model. This scale mismatch is particularly relevant in the Amazon shelf region, where river discharge, mesoscale circulation, and tidal processes generate strong spatial variability.

Quantitatively, the model shows a moderate but significant spatial correlation with CARS for surface nitrate, with $r = 0.51$ and $p < 0.05$, indicating that it captures the dominant regional-scale patterns. The low median absolute error of 0.24 mmol m^{-3} and the limited positive bias of +0.60 mmol m^{-3} suggest reasonable overall agreement, although with a slight tendency to overestimate nitrate concentrations. The larger mean absolute error of 1.33 mmol m^{-3} and root-mean-square error of 5.43 mmol m^{-3} likely reflect localized differences in the position and intensity of nitrate gradients, which are smoothed in CARS but more explicitly represented in the model.

This interpretation is supported by the much larger spatial variability simulated by the model, with a standard deviation of 6.08 mmol m^{-3} compared with 1.77 mmol m^{-3} in CARS. The NOTIDES simulation therefore remains consistent with the large-scale nitrate distribution described by CARS, while providing a higher-resolution representation of fine-scale surface nitrate variability across the Amazon shelf and adjacent offshore waters.

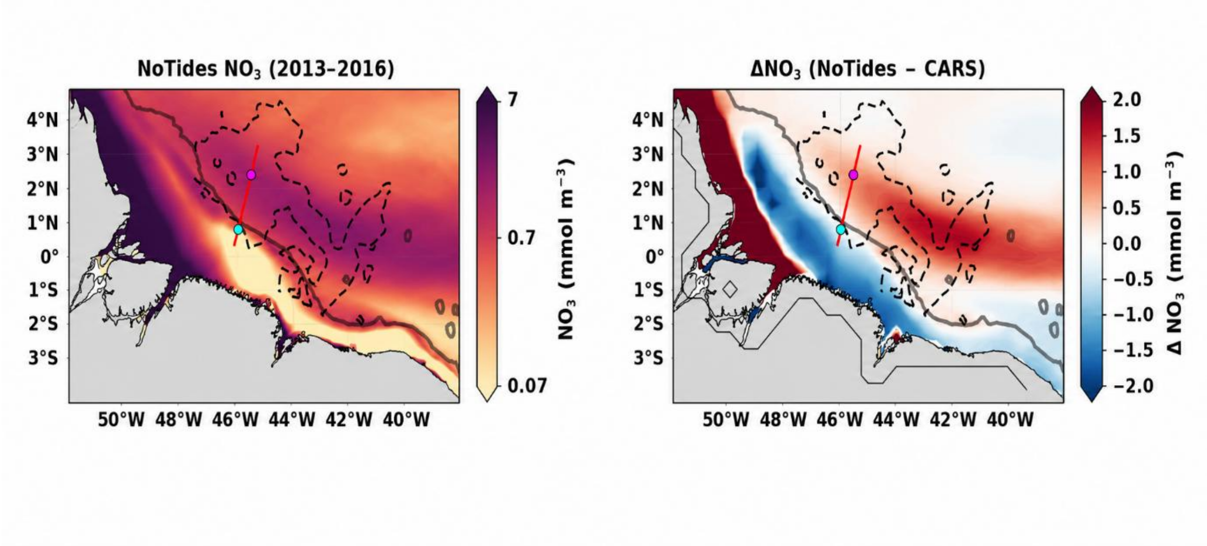

Figure 3 : Spatial distribution of surface nitrate concentration (NO_3^-) in the Amazon shelf-continuum region.(Left) mean nitrate concentration simulated by the NoTides configuration over 2013–2016 (log_{10} scale). (Right) Difference between the NoTides simulation and the CARS climatology (ΔNO_3 = NoTides − CARS).

3.2 Nitrate and Chlorophyll-a vertical profile

A major objective of this study is to assess how tides and internal tides shape nitrate and chlorophyll-a distributions, with particular emphasis on their vertical structure. To this end, we compared modeled nitrate and chlorophyll-a profiles with in situ observations collected during the AMAZOMIX campaign between August and October 2021 along the internal-tide propagation pathway (Figure 2).

The model reproduces the main features of the observed vertical nitrate structure. Both the observations and the simulation show low nitrate concentrations in the upper layer and a well-defined nitracline located between approximately 90 and 160 m depth. As shown in Figure 4, the modeled mean profile and its associated variability remain within the observed range throughout most of the water column. The model nevertheless shows slightly weaker variability than the observations, suggesting a modest smoothing of vertical nitrate fluctuations. Overall, this agreement indicates that the model reliably represents the vertical nitrate structure and supports its use for investigating the effects of tides and internal tides on nutrient distributions.

The chlorophyll-a comparison reveals a distinct vertical structure. Observations show a subsurface chlorophyll maximum at approximately 20–30 m depth, followed by a progressive decrease with depth and low concentrations below about 120 m. The model captures this overall structure reasonably well, including the depth of the chlorophyll maximum, the subsurface decline, and the weak chlorophyll concentrations in deeper waters. The modeled mean profile generally remains within the range of observed variability throughout the water column. However, the simulation tends to underestimate chlorophyll-a concentrations in the upper layer and around/below the deep chlorophyll maximum, indicating that the amplitude of the biological signal is somewhat damped in the model. Despite these differences, the simulated chlorophyll-a structure remains consistent with the observations and provides confidence in the model's ability to represent the vertical organization of phytoplankton biomass along the internal-tide pathway.

Together, these comparisons show that the model captures the main observed vertical gradients of both nitrate and chlorophyll-a. This evaluation supports the use of the coupled physical–biogeochemical configuration to examine how tidal and internal-tide processes modulate nutrient supply and phytoplankton distributions in the Amazon shelf–offshore continuum.

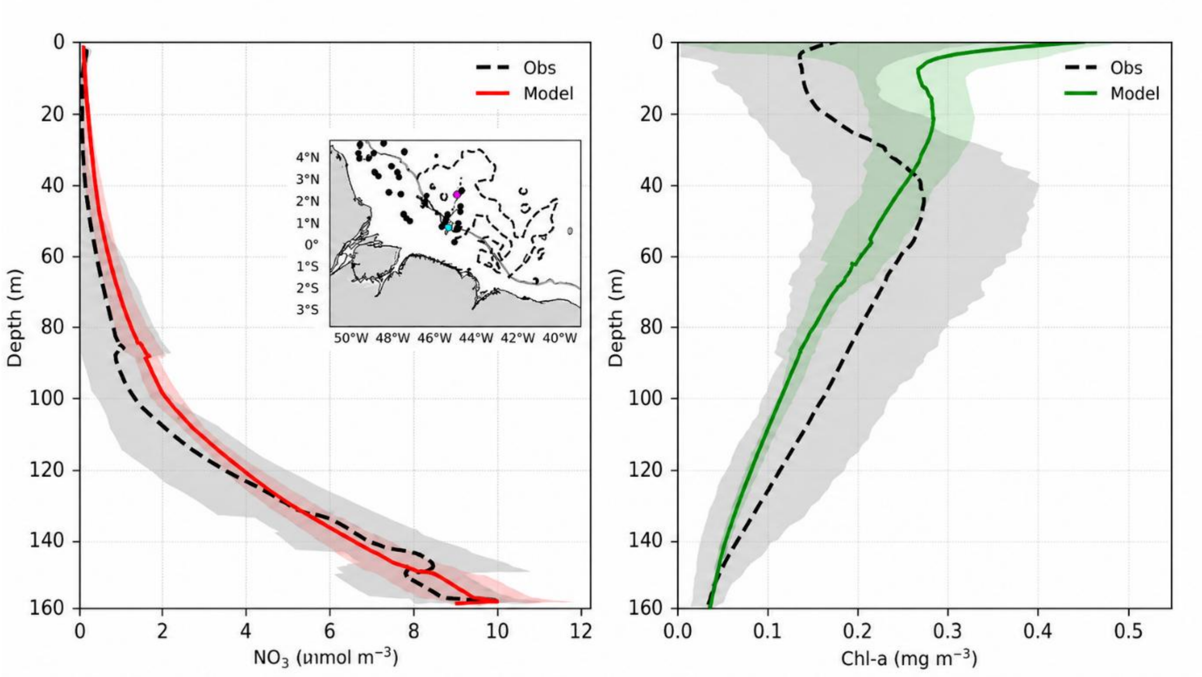

Figure 4 : Comparison model (mean Aug-Sep-Oct 2013-2016) vs Amazomix profiles (Aug - Sep - Oct 2021) of NO3 concentration (mmol NO3 m-3) and Chlorophyll-a (mg CHL-a m-3). Black points correspond to the Amazomix stations

3.3 Chlorophyll-a Mean surface spatial Pattern

The NOTIDES simulation reproduces the same order of magnitude of surface chlorophyll concentrations as the satellite-derived product, with values ranging from approximately 0.08 to 0.5 mg Chl-a m^{-3} over most of the domain (Figure 5, left). The highest concentrations occur over the continental shelf and along the coast, consistent with the influence of riverine nutrient inputs, particularly nitrate, as well as sedimentary and coastal processes. Although the color scale is capped at 1 mg Chl-a m^{-3}, satellite-derived chlorophyll concentrations locally exceed 20–30 mg Chl-a m^{-3} over the shelf. These very high values should be interpreted with caution, as ocean-color retrievals in optically complex coastal waters can be strongly affected by suspended sediments, colored dissolved organic matter, and bottom or shallow-water effects, leading to uncertain chlorophyll estimates (Cardoso dos Santos et al., 2025).

The model captures the marked cross-shelf gradient, with surface chlorophyll concentrations decreasing rapidly from the coastal shelf toward offshore waters. The model–observation differences reveal contrasted regional biases (Figure 5, right). Negative anomalies dominate over the shelf and along the coastal margin, indicating an underestimation of the highest coastal chlorophyll concentrations. In contrast, weak positive anomalies are found offshore and in the equatorial band. Within the region influenced by internal tides, the NOTIDES simulation exhibits a slight positive bias, generally lower than 0.1 mg Chl-a m^{-3}. Given observed concentrations of about 0.3 mg Chl-a m^{-3} in this region, this corresponds to a relative overestimation of approximately 30–35%.

Overall, the comparison with satellite-derived chlorophyll indicates that the model reproduces the large-scale surface chlorophyll distribution well. The spatial correlation is high, with $r = 0.85$ and $p < 0.05$, showing that the simulation captures most of the regional variability. Over the full domain, the model exhibits a moderate negative bias of −0.259 mg Chl-a m^{-3}, indicating a limited overall tendency to underestimate chlorophyll concentrations. Error levels remain moderate, with a mean absolute error of 0.348 mg Chl-a m^{-3} and a median absolute error of 0.088 mg Chl-a m^{-3}, suggesting that much of the domain is represented with reasonable accuracy. The larger root-mean-square error of 1.241 mg Chl m^{-3} points to localized mismatches of greater amplitude, mainly associated with the coastal and shelf regions. In addition, the simulated spatial variability is weaker than in the satellite product, with a standard deviation of 1.502 mg Chl m^{-3} compared with 2.195 mg Chl m^{-3} in the observations, corresponding to an amplitude ratio of 0.68. This indicates that the model tends to smooth the strongest chlorophyll gradients, while preserving the main regional-scale structures.

When the comparison is restricted to the offshore domain north of the 1000 m isobath, model performance improves substantially. In this region, the mean bias becomes nearly negligible, 0.010 mg Chl-a m^{-3}, and absolute errors remain low, with a mean absolute error of 0.094 mg Chl-a m^{-3} and a median absolute error of 0.081 mg Chl m^{-3}. The root-mean-square error is also small, 0.210 mg Chl-a m^{-3}, and very close to the centered root-mean-square error, 0.209 mg Chl m^{-3}, indicating that residual errors are not primarily driven by systematic bias. The spatial correlation reaches 0.90, confirming that the model accurately captures the regional organization of offshore chlorophyll. The simulated variability is, however, somewhat stronger than in the satellite product, with a standard deviation of 0.402 mg Chl-a m^{-3} compared with 0.246 mg Chl-a m^{-3} in the observations, corresponding to an amplitude ratio of 1.63. This suggests that the model enhances offshore chlorophyll contrasts, even though it correctly reproduces their spatial organization.

Taken together, these results show that the model represents offshore surface chlorophyll particularly well, both in magnitude and spatial structure. The larger discrepancies over the full domain mainly arise from coastal and shelf environments, where optical complexity, strong riverine influence, and sharp biogeochemical gradients make both satellite retrievals and model representation more challenging.

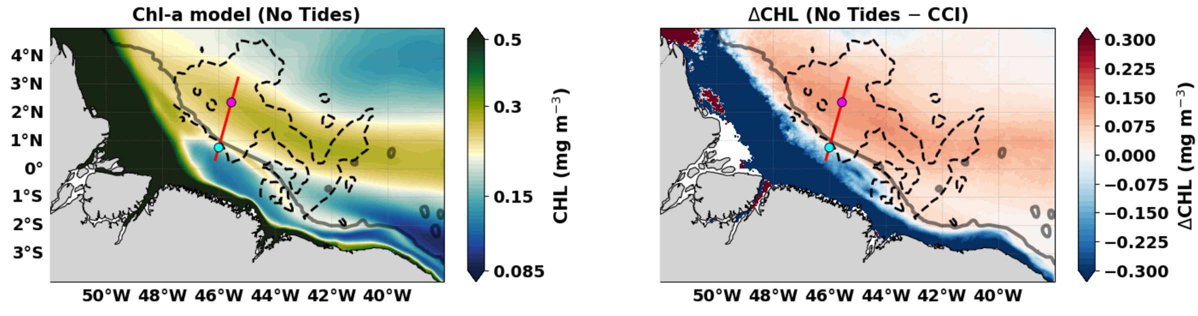

Figure 5: (Left) Mean surface chlorophyll-a field simulated by the model without tides (No Tides), expressed in mg m^{-3} (logarithmic scale), over the western equatorial Atlantic margin. (Right) Difference in chlorophyll-a between the No Tides simulation and CCI satellite observations (ΔCHL = No Tides − CCI).

https://doi.org/10.5194/egusphere-2026-2729
Preprint. Discussion started: 27 May 2026

4. Results

4.1 Tides impact on Chlorophyll-a and Nitrates in the Amazon shelf-open ocean continuum

4.1.1 Mean State – surface map of Nitrates and Chlorophyll-a

The annual mean surface nitrate distribution in the TIDES simulation reveals three main nitrate-rich regions (Figure 6, lower left). The highest concentrations occur over the Amazon shelf, directly offshore of the river mouth, where nitrate exceeds 1 mmol NO_3 m^{-3}. Elevated concentrations are also simulated along the shelf break, with values ranging from about 0.3 to 0.6 mmol NO_3 m^{-3} and local maxima near the main internal-tide generation sites. A third nitrate-rich region appears along the equatorial band, which overlaps with the internal-tide propagation pathway and where nitrate concentrations remain close to 0.4 mmol NO_3 m^{-3}. Together, these patterns identify the main regions where surface nutrient availability is enhanced by the combined influence of riverine inputs, shelf processes, and equatorial dynamics. The annual mean surface chlorophyll-a distribution broadly follows the nitrate pattern (Figure 6, upper left). The highest chlorophyll-a concentrations are found over the Amazon shelf, directly offshore of the river mouth, where values exceed 0.5 mg Chl-a m^{-3}. Enhanced chlorophyll-a concentrations are also simulated along the equatorial band, suggesting a possible contribution from equatorial upwelling, while concentrations along the shelf break remain higher than in the surrounding offshore waters. This spatial correspondence between nitrate and chlorophyll-a indicates that regions of enhanced nutrient availability generally sustain higher surface phytoplankton biomass. The TIDES − NOTIDES anomalies reveal that tidal effects are strongest in the main biogeochemically active regions: offshore of the Amazon mouth, along the shelf break, and within the internal-tide propagation band (Figure 6, right panels). The nitrate response is particularly pronounced. Tides increase surface nitrate by about 0.2–0.4 mmol NO_3 m^{-3} over the northern shelf, along the shelf break, and within the internal-tide propagation band, locally corresponding to relative increases of about 50% or more compared with the NOTIDES simulation. These positive anomalies are consistent with enhanced vertical exchanges driven by barotropic tidal dissipation and internal-tide breaking, which can promote the upward supply of subsurface nitrate into the euphotic layer (Assene et al., 2024). By contrast, negative nitrate anomalies of about −0.2 to −0.4 mmol NO_3 m^{-3} occur mainly over the southern shelf and nearshore regions. In these shallow waters, which are strongly influenced by riverine inputs, tidal mixing may dilute the nitrate-rich surface plume by enhancing exchanges with relatively nitrate-poor subsurface waters. A similar tide-induced vertical redistribution mechanism was previously identified for temperature over the Amazon shelf by Assene et al. (2024). The chlorophyll-a response is weaker and more spatially heterogeneous than the nitrate response. Tides reduce surface chlorophyll-a by up to about 0.2 mg Chl-a m^{-3} directly offshore of the Amazon mouth, corresponding to a local decrease of roughly 30–40% relative to the NOTIDES simulation. Farther offshore, tides generally enhance chlorophyll-a, with positive anomalies of about 0.05–0.15 mg Chl-a m^{-3}. This offshore increase suggests that tidally supplied nitrate can stimulate phytoplankton biomass where light conditions are more favorable and plume-related turbidity is weaker. Overall, these results show that tides substantially reshape surface nitrate availability over the Amazon shelf–offshore continuum. The chlorophyll-a response, however, is more complex because it reflects not only nutrient supply, but also advection, vertical mixing, light availability, and biological adjustment timescales near the river plume.

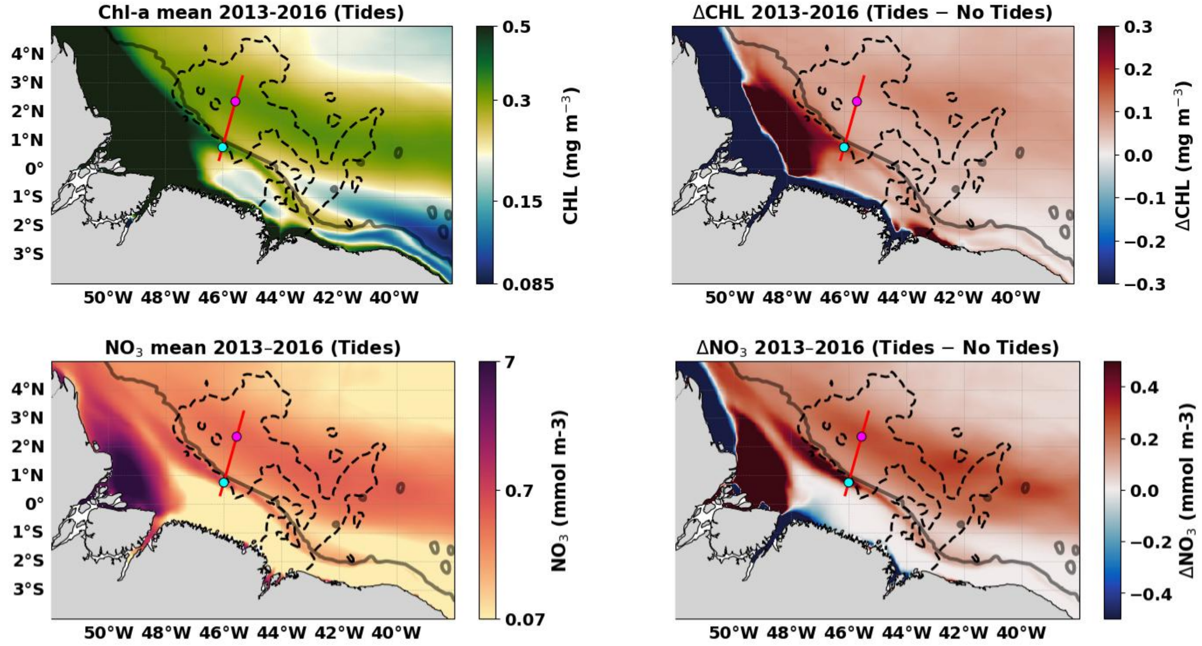

Figure 6 : Spatial distribution of surface Chlorophyll-a (Chl-*a*; top row) and nitrate (NO_3; bottom row) concentrations and tidal impact over the Amazon shelf region. The left panel shows the annual mean (2013-2016) surface chlorophyll-a and nitrate concentrations simulated in the TIDES experiment. The right panel displays the corresponding difference ΔCHL and ΔNO3 (TIDES − NOTIDES), highlighting the net impact of tidal processes on surface chlorophyll-a and nitrate concentrations.

4.1.2 Mean State along the Internal-Tide Pathway – Transect A

The annual mean vertical distributions of chlorophyll-a and nitrate along the internal-tide propagation transect reveal a clear vertical structuring of the biogeochemical fields (Figure 7). Chlorophyll-a is organized into three main layers. The upper layer, extending from the surface to approximately 50 m depth, is characterized by relatively high concentrations, on the order of 0.3 mg Chl-a m^{-3}. Within this layer, a subsurface chlorophyll maximum, hereafter referred to as the deep chlorophyll maximum, is located around 25 m depth. This maximum is particularly well developed near the internal-tide-influenced sites P1 and P2, suggesting a localized subsurface accumulation of phytoplankton biomass along the internal-tide pathway. Below this chlorophyll-rich layer, a transition zone extends from about 50 to 100 m depth, where chlorophyll-a concentrations decrease to approximately 0.20 mg Chl-a m^{-3}. Beneath roughly 150 m, chlorophyll-a concentrations become very low, generally ranging between 0 and 0.05 mg Chl-a m^{-3}, consistent with depths where light availability is insufficient to sustain significant photosynthetic activity. Nitrate exhibits an opposite vertical structure. Surface nitrate concentrations remain low in the upper layer, consistent with phytoplankton uptake within the euphotic zone. Below this nutrient-depleted surface layer, the nitracline extends approximately between 90 and 160 m depth, marking the depth range over which nitrate concentrations increase sharply. Beneath the nitracline, nitrate accumulates in deeper waters where phytoplankton consumption is weak and remineralization processes replenish the nutrient pool. A marked nitrate enrichment is observed near the main internal-tide generation site, consistent with enhanced chlorophyll-a concentrations in the overlying layers.

The comparison between the TIDES and NOTIDES simulations reveals a clear tidal imprint on this vertical structure. In the nitrate field, tides induce a pronounced vertical redistribution, with nitrate decreasing by up to about 2 mmol NO_3 m^{-3} below the nitracline and increasing by a similar magnitude within the nitracline, between the dashed white and magenta curves in Figure 7. This dipolar anomaly strongly suggests an upward transfer of nitrate associated with tidal processes. The signal is particularly evident near the internal-tide generation site and along the offshore propagation pathway. The chlorophyll-a response is also vertically structured. Tides induce negative chlorophyll-a anomalies near the nitracline, while positive anomalies develop in the upper euphotic layer. This pattern indicates an upward redistribution of phytoplankton biomass and/or a biological response to tidally supplied nitrate reaching illuminated waters. Surface chlorophyll-a enrichment is not spatially uniform, but is concentrated in two main regions: near the internal-tide generation site, where anomalies reach about +0.15 mg Chl-a m^{-3}, and around station P2, where the chlorophyll-a increase coincides with an upward displacement of nitrate isolines. This local shoaling of nitrate surfaces suggests nitrate uplift in the main offshore dissipation region.

Taken together, the nitrate and chlorophyll-a anomalies indicate that tides reshape the vertical coupling between nutrient supply and phytoplankton biomass. By lifting nitrate toward the upper nitracline and the euphotic layer, internal tides promote localized chlorophyll-a increases along the propagation pathway, especially near the generation and offshore dissipation regions.

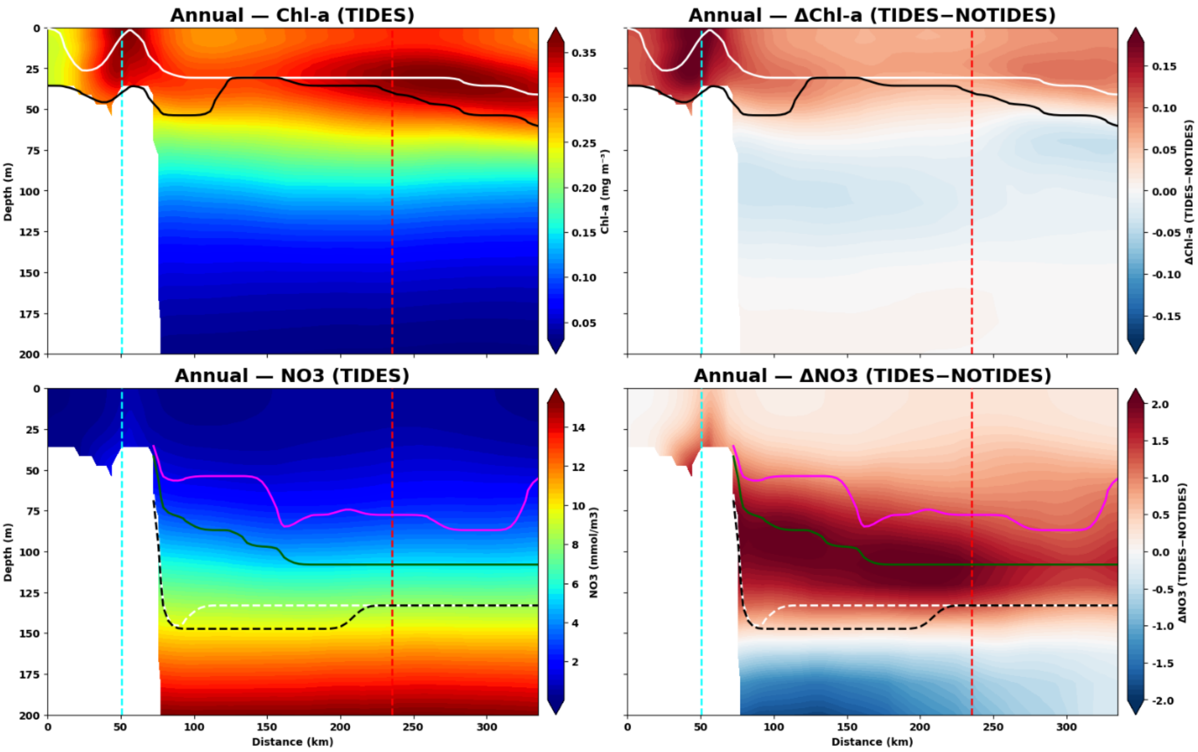

Figure 7. Annual mean vertical transects of chlorophyll-*a* (Chl-*a*; top row) and nitrate (NO_3; bottom row) along the internal tide (IT) propagation transect across the Amazon shelf-open ocean continuum. The left panels show the simulation including tides (TIDES), while the right panels show the tidal contribution, computed as the difference between the simulations with and without tides (Δ = TIDES − NOTIDES). The magenta and green lines indicate the nitracline depth in the TIDES and NOTIDES simulations, respectively. The white and black lines indicate the depth of the deep chlorophyll maximum (DCM) in the TIDES and NOTIDES simulations, respectively. The blue and red vertical dashed lines indicate the tide generation site and the P2 site, respectively.

4.1.3. Seasonal variability

The seasonal surface distributions of nitrate and chlorophyll-a during April–May–June (AMJ) and August–September–October (ASO) are shown in Figure 8. In both seasons, the large-scale spatial organization remains broadly consistent with the annual mean pattern (Figure 6), with enhanced concentrations over the northern Amazon shelf, lower values over the southern shelf, and elevated offshore concentrations along the equatorial band and the internal-tide propagation region. However, both the background biogeochemical fields and the tidal response exhibit marked seasonal contrasts. The nitrate distribution highlights the seasonal modulation of nutrient availability across the Amazon shelf–offshore continuum. In both AMJ and ASO, nitrate concentrations are enhanced over the northern shelf, along the shelf break, and within the equatorial internal-tide propagation band. Compared with AMJ, ASO is characterized by higher offshore nitrate concentrations, particularly along the equatorial band, suggesting a seasonal reinforcement of nutrient availability in the open-ocean region. By contrast, nitrate concentrations over the shelf remain strongly influenced by riverine inputs and shelf processes, leading to marked spatial gradients between the northern and southern shelf. The chlorophyll-a distribution broadly follows these nutrient patterns, although with a more spatially heterogeneous response. Concentrations over the northern shelf and offshore of the Amazon mouth remain high in both seasons, generally exceeding 0.3 mg Chl-a m^{-3}. The offshore equatorial band shows a pronounced seasonal signal, with lower chlorophyll-a concentrations during AMJ and higher values during ASO, broadly consistent with the seasonal enhancement of offshore nitrate availability. The chlorophyll-rich region offshore of the Amazon mouth also appears more spatially confined during ASO than during AMJ, indicating a seasonal reorganization of the plume-influenced region. The TIDES − NOTIDES anomalies show that tidal effects remain concentrated in the same key regions identified in the annual mean fields: offshore of the Amazon mouth, along the shelf break, and within the internal-tide propagation band. The nitrate response to tides is stronger during AMJ than during ASO. Positive nitrate anomalies reach about +2.5 mmol NO_3 m^{-3} in AMJ, compared with about +1.5 mmol NO_3 m^{-3} in ASO, with maximum values located over the northern shelf and near the internal-tide generation region. In both seasons, the tidal nitrate signal remains weak over the southern shelf, consistent with the north–south asymmetry already identified in the annual mean fields. This stronger AMJ response indicates that tidal processes enhance nutrient availability more efficiently when the upper-ocean structure favors nitrate uplift. The chlorophyll-a response to tides follows this nutrient redistribution but is more heterogeneous. In both seasons, tides induce a dipolar horizontal response, with a decrease near the coast and an enrichment farther offshore over the outer plume region. This contrast is stronger in AMJ than in ASO. Offshore chlorophyll-a anomalies reach about +0.10 mg Chl-a m^{-3} in AMJ, compared with about +0.05 mg Chl-a m^{-3} in ASO, while negative anomalies of comparable magnitude occur closer to the coast. This pattern suggests that tidal processes contribute to a seasonal redistribution of phytoplankton biomass from the nearshore plume region toward offshore waters and/or stimulate offshore growth where tidally supplied nitrate reaches better-lit waters. This seasonal contrast is further supported by the vertical structure along the internal-tide propagation transect (Figure 9). The nitrate field shows a clear seasonal displacement of the nitracline. In AMJ, the nitracline is shallower, starting at about 50–60 m and extending down to roughly 130–150 m. In ASO, it shifts downward and typically extends from about 80–100 m to 150 m depth. This deeper nitracline in ASO likely reduces the efficiency with which tides can uplift nitrate into the upper water column. The chlorophyll-a field responds consistently with this nutrient structure: in AMJ, it exhibits a more pronounced deep chlorophyll maximum, whereas in ASO the vertical chlorophyll-a structure is smoother and less sharply peaked. The TIDES − NOTIDES vertical sections confirm that tides tend to shoal both the nitracline and the deep chlorophyll maximum. In both seasons, tides generate a dipolar nitrate anomaly, with nitrate enrichment within the nitracline and depletion below it, consistent with an upward redistribution of nutrients. This redistribution is stronger and shallower in AMJ, when positive nitrate anomalies extend upward toward the base of the surface layer and coincide with a more pronounced chlorophyll-a response.

In the chlorophyll-a field, tides induce a decrease in the intermediate layer and an increase in the upper euphotic layer in both seasons, indicating an upward redistribution of phytoplankton biomass and/or enhanced growth where tidally supplied nitrate reaches illuminated waters. The amplitude of this vertical redistribution is larger in AMJ: surface chlorophyll-a anomalies reach about +0.10 to +0.15 mg Chl-a m^{-3}, compared with about +0.05 to +0.07 mg Chl-a m^{-3} in ASO. Conversely, the intermediate chlorophyll-a decrease is also stronger in AMJ. Taken together, these results indicate that the shallower nitracline during AMJ allows tidal uplift to deliver nitrate more efficiently toward the euphotic layer, thereby strengthening the surface chlorophyll-a response. In ASO, the deeper nitracline limits this tidal nutrient supply, resulting in a weaker biological response. This seasonal modulation is consistent with previous studies emphasizing the role of Amazon River plume dynamics and associated stratification in shaping the regional seasonal cycle (Assene et al., 2024; Tchilibou et al., 2022).

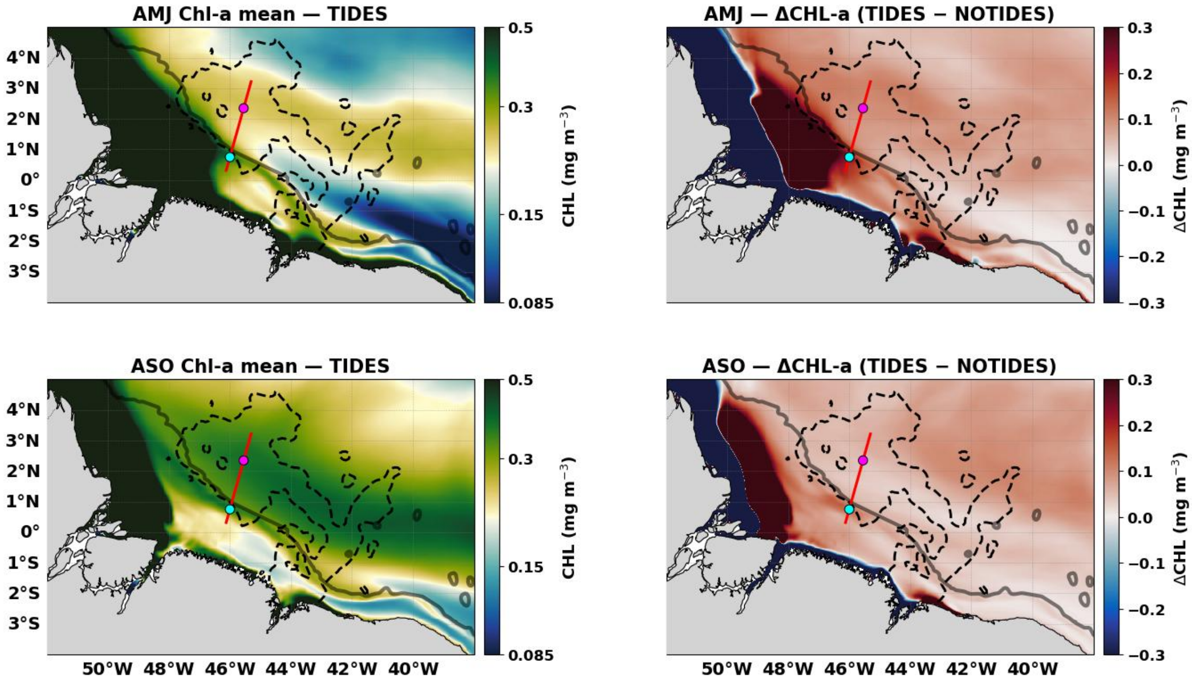

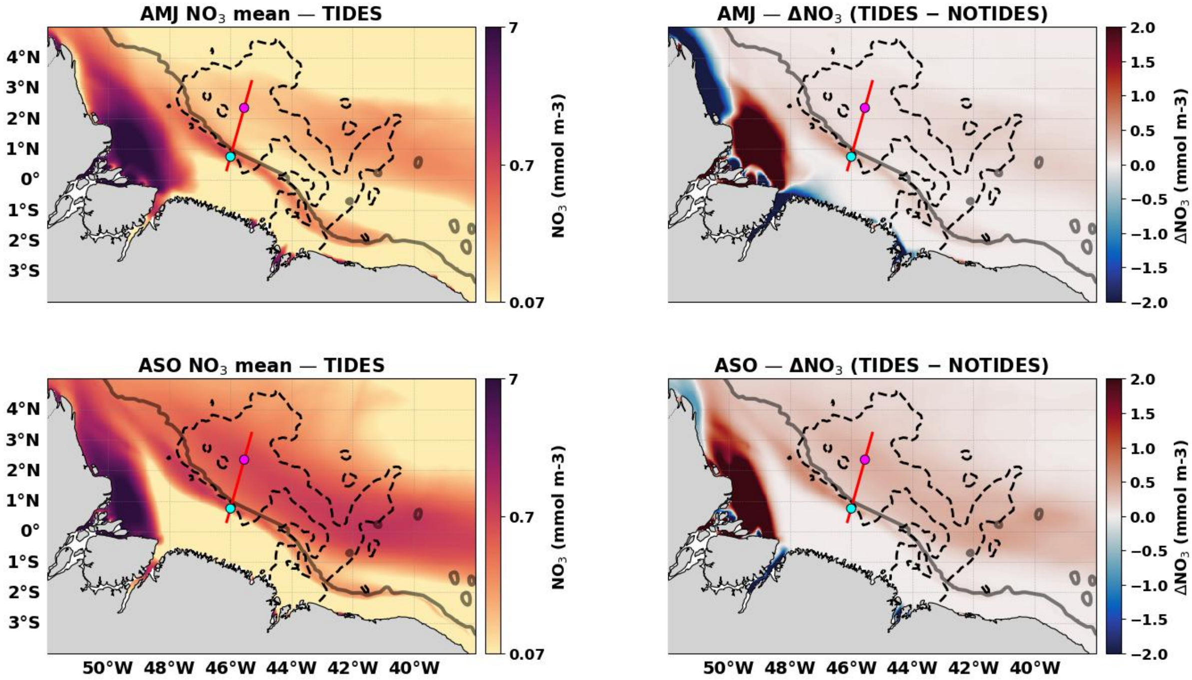

Figure 8 : Seasonal distribution of surface Chl-a and Nitrate concentration over the Amazon shelf. Panels show the seasonal mean surface Chl-a during April May June (top row) and August September October (bottom row). Left panels display CHL simulated in the TIDES experiment, while right panels show the corresponding difference ΔCHL = TIDES − NOTIDES.

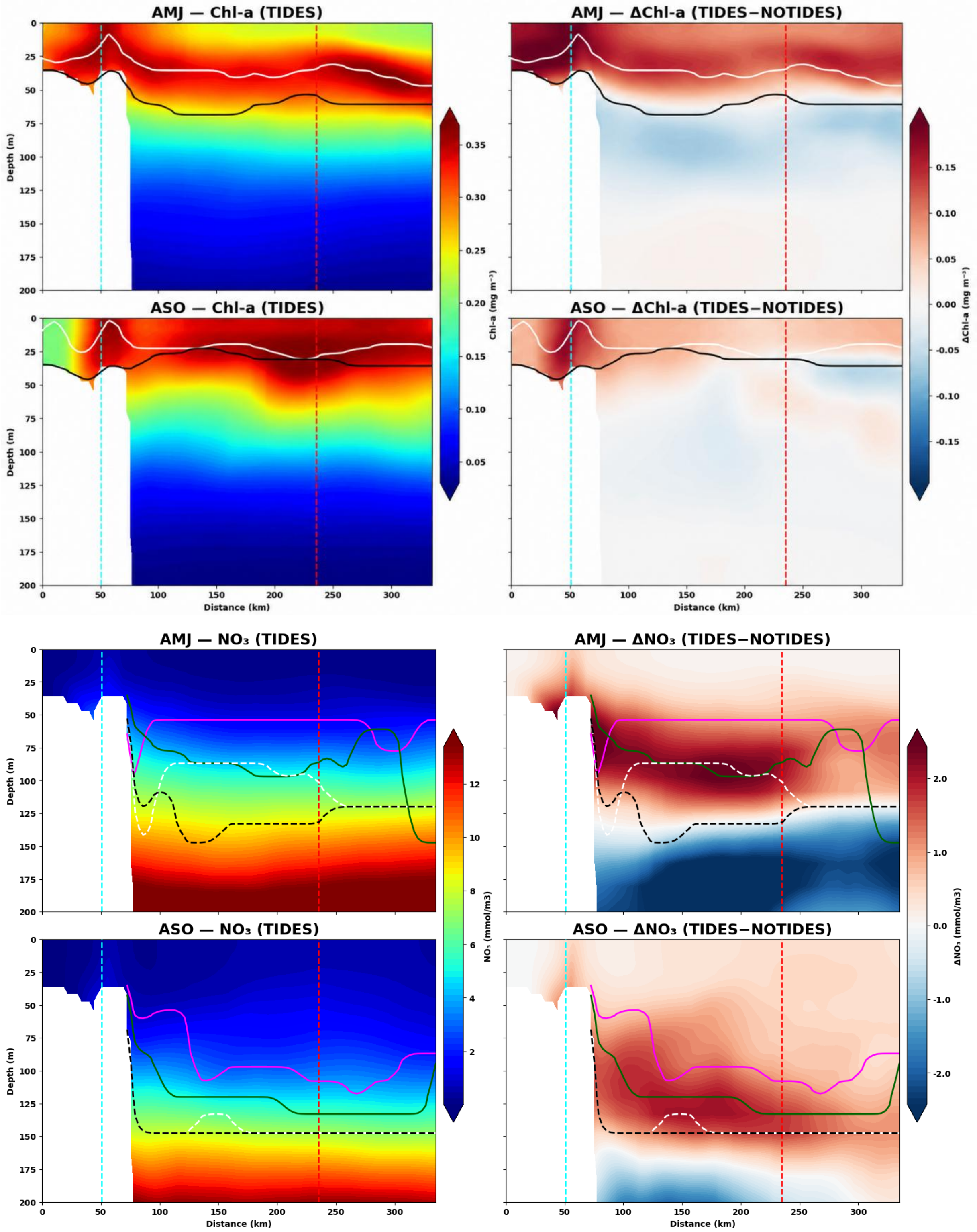
AMJ — Chl-a (TIDES)
AMJ — ΔChl-a (TIDES−NOTIDES)
ASO — Chl-a (TIDES)
ASO — ΔChl-a (TIDES−NOTIDES)
Depth (m)
Distance (km)
Chl-a (mg m⁻³)
0.35
0.30
0.25
0.20
0.15
0.10
0.05
ΔChl-a (mg m⁻³)
0.15
0.10
0.05
0.00
-0.05
-0.10
-0.15
AMJ — NO₃ (TIDES)
AMJ — ΔNO₃ (TIDES−NOTIDES)
ASO — NO₃ (TIDES)
ASO — ΔNO₃ (TIDES−NOTIDES)
NO₃ (mmol/m3)
12
10
8
6
4
2
ΔNO₃ (mmol/m3)
2.0
1.0
0.0
-1.0
-2.0
0
25
50
75
100
125
150
175
200
0
50
100
150
200
250
300

https://doi.org/10.5194/egusphere-2026-2729
Preprint. Discussion started: 27 May 2026

Figure 9. Seasonal mean vertical transects of chlorophyll-*a* (Chl-*a*, upper panels) and nitrate (NO_3, lower panels) across the Amazon shelf for April–May–June (AMJ; upper rows) and August–September–October (ASO; lower rows). For each variable and season, the left panels show the simulations including tides (TIDES), whereas the right panels show the tidal contribution, estimated as the difference between the simulations with and without tides (Δ = TIDES − NOTIDES). In the Chl-*a* panels, the white and black lines indicate the depth of the deep chlorophyll maximum (DCM) in the TIDES and NOTIDES simulations, respectively. In the NO_3 panels, the magenta and green lines indicate the upper nitracline depth in the TIDES and NOTIDES simulations, respectively. The dashed white and dashed black lines indicate the lower nitracline depth in the TIDES and NOTIDES simulations, respectively.

4.1.4 Seasonal contrast and tidal contribution to seasonal variability

The objective here is to distinguish the respective contributions of seasonal variability and tidal forcing to the observed seasonal changes in surface chlorophyll-a and nitrate. The seasonal differences between April–May–June (AMJ) and August–September–October (ASO) reveal broadly similar spatial patterns for both variables (Figure 10). Over the Amazon shelf, chlorophyll-a and nitrate concentrations are higher during AMJ than during ASO, with increases of approximately 0.3 mg Chl-a m^{-3} and 0.4 mmol NO_3 m^{-3}, respectively. This shelf enrichment is consistent with the seasonal evolution of Amazon River discharge, as the onset of the flood season enhances nutrient delivery to the shelf and promotes phytoplankton development. In contrast, the offshore oceanic region shows the opposite seasonal behavior. During AMJ, chlorophyll-a and nitrate concentrations are lower than during ASO, with decreases of about 0.15 mg Chl-a m^{-3} and 0.5 mmol NO_3 m^{-3}, respectively. The total seasonal contrast is therefore spatially heterogeneous, with enrichment over the shelf and relative depletion offshore. When the tidal contribution to this seasonal contrast is isolated, a distinct cone-shaped pattern emerges. The strongest chlorophyll-a signal occurs along the shelf break, near the main internal-tide generation site, where anomalies reach about 0.15 mg Chl-a m^{-3}. Farther offshore, north of the shelf, a stronger positive anomaly develops, reaching approximately 0.3 mg Chl-a m^{-3}. In contrast, a negative anomaly of comparable magnitude is found over the northern coastal shelf. This dipolar pattern is consistent with the AMJ TIDES − NOTIDES difference identified previously and suggests that tides reinforce the seasonal redistribution of chlorophyll-a from the coastal shelf toward the offshore plume-influenced region. Offshore, a positive chlorophyll-a anomaly of about 0.1 mg Chl-a m^{-3} extends across the internal-tide propagation region, indicating that tidal effects are particularly strong during AMJ in the open-ocean propagation zone. The nitrate response differs from that of chlorophyll-a. In the tidal seasonal-difference field, AMJ is associated with a stronger nitrate drawdown of about 0.2 mmol NO_3 m^{-3}, likely reflecting enhanced phytoplankton consumption where tidally supplied nutrients stimulate biological uptake. Thus, the tidal nitrate signal does not simply represent nutrient enrichment; it reflects the combined effects of upward nitrate supply, redistribution, and biological consumption.

A key result is that the spatial structure of the tidal contribution closely resembles that of the total seasonal difference, although with weaker amplitude. This similarity indicates that tides significantly modulate the seasonal biogeochemical cycle of the Amazon shelf–offshore continuum. Quantitatively, the seasonal tidal contribution, estimated as the ratio between the tide-induced seasonal anomaly and the total seasonal anomaly, accounts on average for approximately 63% of the seasonal variability in surface nitrate over the study area. In other words, the tidal effect alone represents more than half of the total seasonal nitrate signal, highlighting the major role of tidal forcing in controlling the seasonal cycle of nutrient availability in the Amazon shelf region.

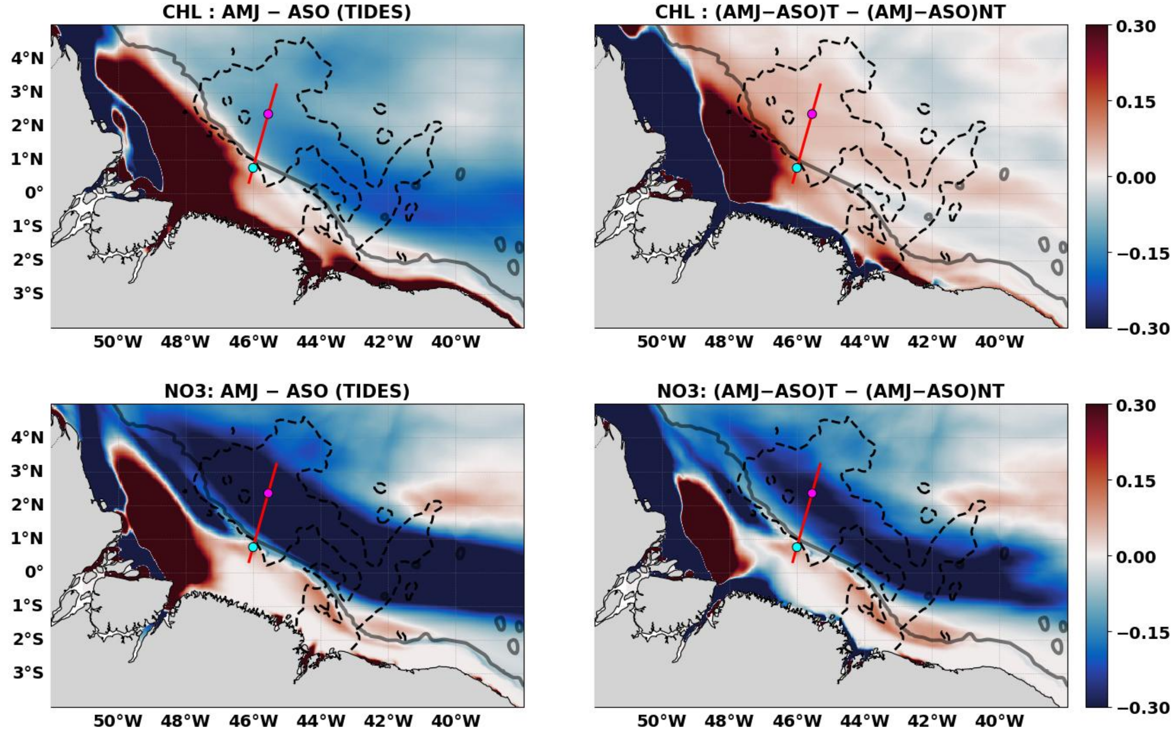

Figure 10 : Seasonal comparison of tidal effects on surface chlorophyll-a (mg Chl-a m-3) and nitrate (mmol NO3 m-3). Left panels show the seasonal difference between AMJ and ASO under the TIDES simulation (AMJ − ASO). Right panels display the difference of seasonal contrasts between the TIDES and NOTIDES simulations: (AMJ − ASO)_T − (AMJ − ASO)_NT. Positive values indicate regions where the inclusion of tides enhances the seasonal contrast between AMJ and ASO, while negative values indicate a reduction of this seasonal contrast. The dashed black line represents the M2 tidal amplitude contour of 1.8 m. The red line represents the transect A

4.2 Spring Neap Tides cycles signature on chlorophyll-a and nitrate concentrations

The previous sections focused on the effect of tides on the mean distribution of chlorophyll-a and nitrate. We now examine the variability associated with the spring–neap tidal cycle, represented by the lunisolar synodic fortnightly tidal constituent MSf, with a period of 14.77 days. In the model, a wavelet analysis was performed in the 14.27–15.27 day period band at the

https://doi.org/10.5194/egusphere-2026-2729
Preprint. Discussion started: 27 May 2026

depth of the deep chlorophyll maximum. The same analysis was applied to the observational chlorophyll product to provide an independent reference, although the observational signal does not necessarily correspond to the exact same sampling depth as the model deep chlorophyll maximum. At the depth of the deep chlorophyll maximum, the TIDES simulation reveals a strong and spatially coherent chlorophyll-a signal in the spring–neap band (Figure 11). Despite differences in sampling depth, both the TIDES simulation and the observations exhibit a distinct cone-shaped pattern, consistent with the spatial structure previously identified in Figure 10. This pattern is organized into two main branches. The first follows the shelf break near the internal-tide generation region, where wavelet power exceeds 12 (mg Chl-a m^{-3})^2 in both the TIDES simulation and the observations, while remaining below 5 (mg Chl-a m^{-3})^2 in the NOTIDES simulation. The second branch extends offshore toward the downstream limit of the baroclinic sea-surface-height signature, where wavelet power reaches about 9 (mg Chl-a m^{-3})^2 in the TIDES simulation and about 11 (mg Chl-a m^{-3})^2 in the observations. The agreement between the TIDES simulation and the observations, together with the absence of this coherent structure in NOTIDES, indicates that the spring–neap chlorophyll-a variability is primarily driven by tidal dynamics. The TIDES − NOTIDES difference further emphasizes this contribution, with positive anomalies exceeding 5 (mg Chl-a m^{-3})^2. Enhanced variability is also found along the pathway of the baroclinic energy flux, showing that the tidal imprint is not confined to the generation site but extends downstream across the internal-tide propagation region. The spectral analysis confirms that the spring–neap band represents a major component of chlorophyll-a variability. At both the internal-tide generation site and site P2, the chlorophyll-a spectra display a clear peak within the spring–neap band (Figure 11, bottom). The amplitude of this peak reaches about 6 (mg Chl-a m^{-3})^2 near the generation site and about 3 (mg Chl-a m^{-3})^2 at P2. A slight shift of the dominant peak toward periods close to 18 days is also observed; this feature is addressed in the Discussion. These peaks are absent from the NOTIDES simulation, confirming their tidal origin. Additional spectral peaks, visible only in the TIDES simulation, occur at 2×MSf and 3×MSf. Their presence further supports the tidal origin of the chlorophyll-a response and suggests that nonlinear or higher-order tidal modulation contributes to phytoplankton variability. Overall, the wavelet and spectral analyses show that tides imprint a coherent spring–neap rhythm on chlorophyll-a variability, extending from the shelf-break generation region toward the offshore internal-tide propagation pathway.

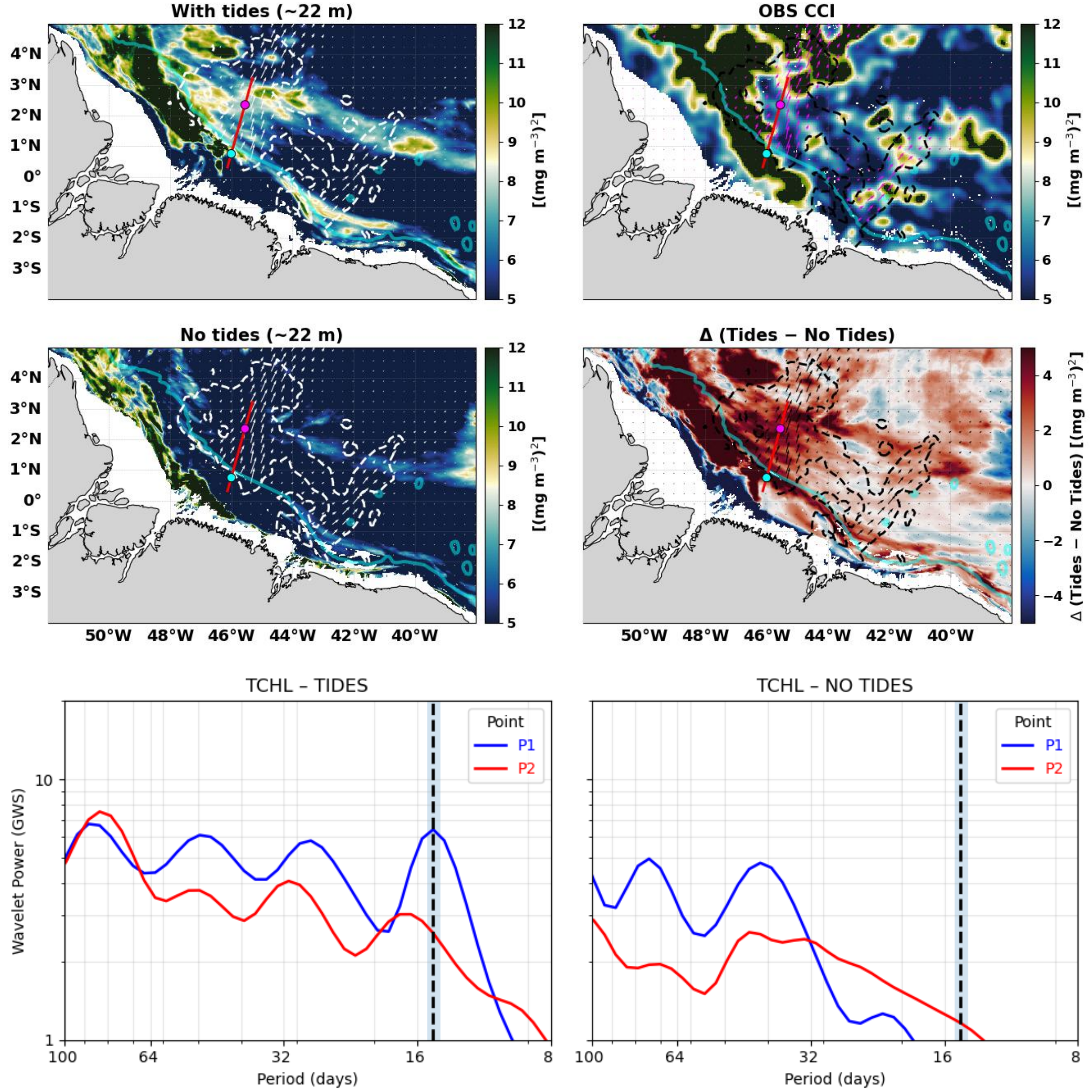

Figure 11: Spatial distribution of spring–neap variability in total chlorophyll-a off the Amazon shelf, expressed as wavelet power in the 14.77-day band at the depth of the deep chlorophyll maximum (DCM). The top panels show the wavelet power from the TIDES simulation, left, and from CCI satellite observations, right. The middle panels show the wavelet power from the NOTIDES simulation, left, and the TIDES − NOTIDES difference, right. The bottom panels show chlorophyll-a wavelet power spectra at the DCM for sites P1 and P2 in the TIDES simulation, left, and the NOTIDES simulation, right.

The spring–neap signal in nitrate concentration at the depth of the deep chlorophyll maximum (DCM) displays a spatial structure that closely resembles the chlorophyll-a signal at the same depth (Figures 11 and 12). A clear cone-shaped pattern appears along the shelf break, with nitrate wavelet power reaching about 1.0–1.2 (mmol NO$_3$ m^{-3})^2 near the internal-tide generation region. A second branch extends offshore toward the downstream limit of the baroclinic sea-surface-height signature, where values range from about 0.8 to 1.0 (mmol NO$_3$ m^{-3})^2.

Enhanced nitrate variability is not restricted to this cone-shaped structure. It also extends along the pathway of the baroclinic energy flux, indicating that the tidal imprint propagates throughout the internal-tide pathway. This spatial organization suggests a direct physical control of nitrate by internal-tide dynamics. As internal tides are generated and propagate offshore, they modify the vertical structure of the water column through vertical displacements and diapycnal mixing, thereby promoting an upward redistribution of nitrate.

More broadly, nitrate wavelet power in the TIDES simulation is up to twice as large as in NOTIDES within both the cone-shaped structure and the downstream propagation region. At site P1, the nitrate spectra show two dominant peaks at the MSf and 2×MSf frequencies, with power values of about 10 (mmol NO$_3$ m^{-3})^2. These peaks remain visible at site P2, although with lower amplitudes, on the order of 1 (mmol NO$_3$ m^{-3})^2. A slight frequency shift, similar to that identified for chlorophyll-a, is also observed at P2.

Together, these results show that nitrate variability is strongly modulated by the spring–neap tidal cycle near the internal-tide generation site, and that this signal remains detectable farther offshore along the internal-tide propagation pathway.

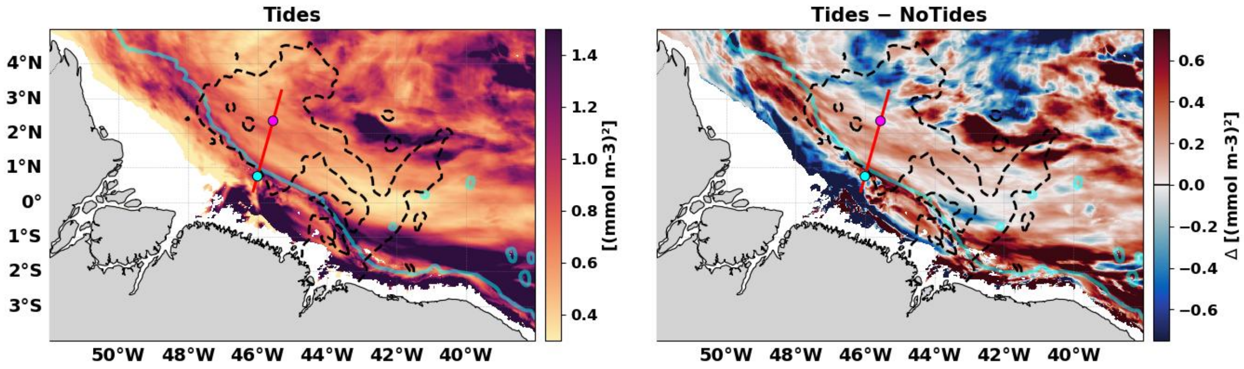

https://doi.org/10.5194/egusphere-2026-2729
Preprint. Discussion started: 27 May 2026

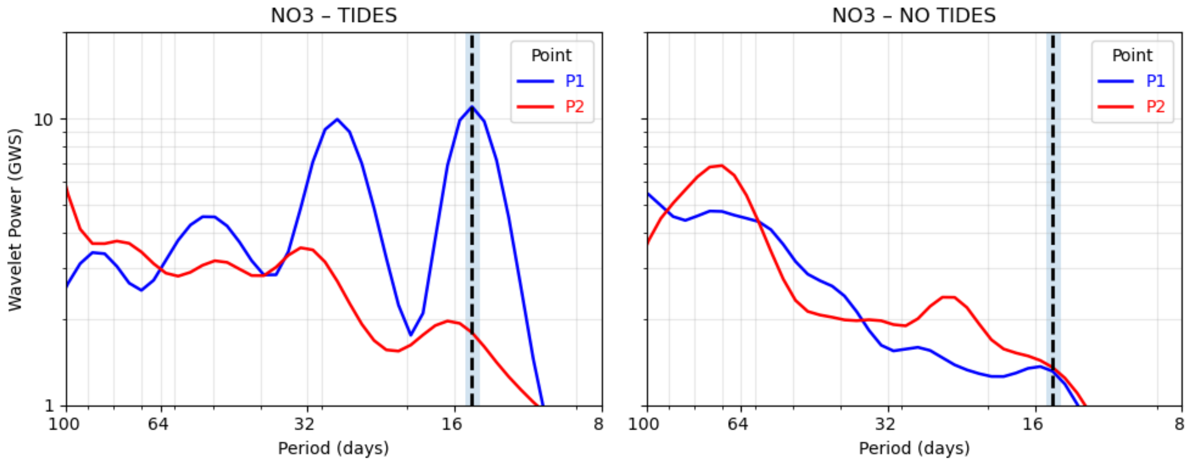

Figure 12 : Spatial distribution of the spring–neap (14.77-day) nitrate signal from wavelet analysis. The map shows the TIDES output (up left) and the difference between simulations TIDES and NO-TIDES (up right), highlighting the tidal contribution in nitrate variability. , bottom row left the TIDES wavelet power and bottom row right the NOTIDES wavelet power at P1 , P2 at DCM for nitrates.

The vertical transects of wavelet power in the 14.27–15.27-day band provide additional insight into the vertical and along-path structure of the spring–neap signal along the internal-tide pathway (Figure 13). In the chlorophyll-a field, two distinct maxima are identified within the deep chlorophyll maximum, with wavelet power exceeding 4 (mg Chl-a $m^{-3})^2$. The first maximum is located near the shelf break, close to the internal-tide generation region, whereas the second occurs farther offshore at site P2, near the maximum of baroclinic sea-surface-height variability. These two features are separated by approximately 190 km, a distance consistent with the expected scale of the first baroclinic mode in the region. Importantly, both chlorophyll-a maxima remain confined to the deep chlorophyll maximum. This indicates that the spring–neap modulation of chlorophyll-a primarily affects the subsurface biomass maximum, rather than the entire upper water column. In contrast, nitrate variability extends over a broader portion of the transect and across a larger vertical range. However, a chlorophyll-a response is detected only where the tidally induced nitrate signal reaches the base of the nitracline and the lower euphotic layer. This suggests that spring–neap nitrate variability can affect phytoplankton biomass only when tidal motions lift nitrate sufficiently upward to influence nutrient supply near the deep chlorophyll maximum. In regions where this vertical connection is established, nitrate wavelet power reaches values on the order of 8 (mmol NO_3 $m^{-3})^2$, highlighting the strength of the tidal nutrient signal relative to the chlorophyll-a response. The TIDES − NOTIDES comparison confirms that tides are responsible for the signatures observed both near the shelf break and at site P2. Beyond these two main chlorophyll-a hotspots, nitrate variability displays an oscillatory vertical pattern, alternating between upward and downward excursions along the section. This structure follows the internal-tide energy propagation pathway and suggests that the biogeochemical response is dynamically constrained by the internal-tide field, rather than being limited to the generation region alone.

This interpretation is consistent with previous evidence of mode-1 internal-tide energy propagation along the same transect (Kouogang et al., 2025a).

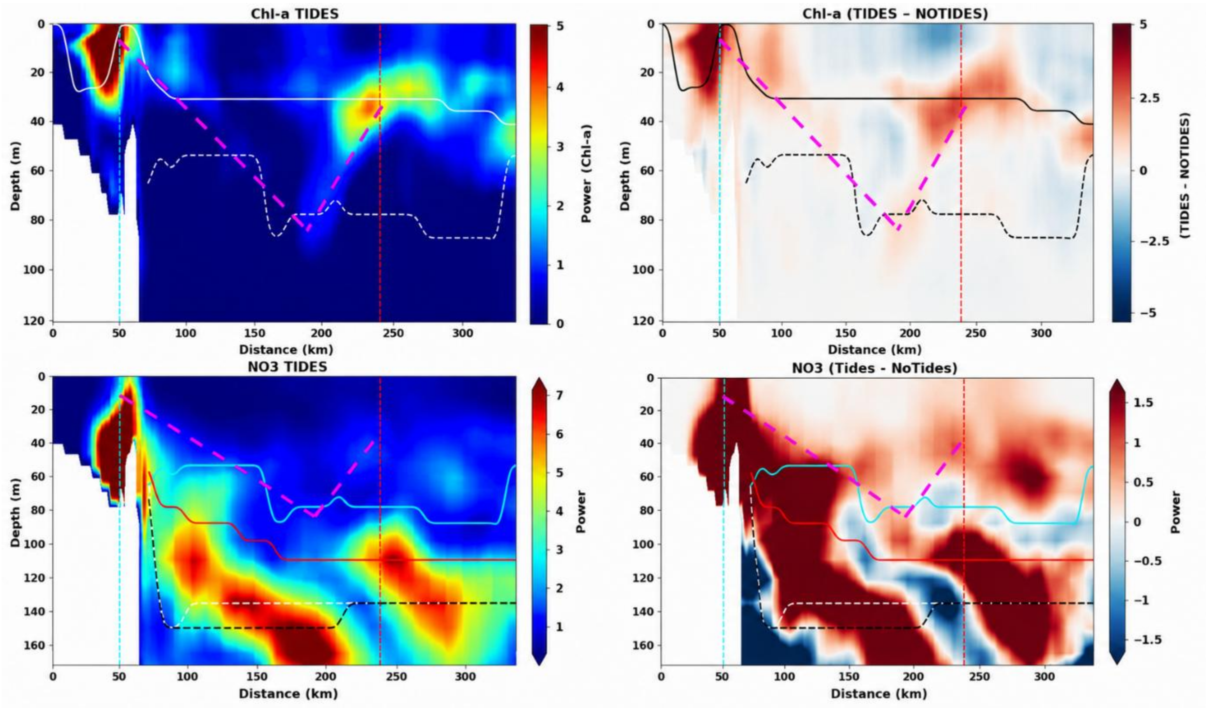

Figure 13 : Vertical distribution of the spring–neap signal along the internal-tide pathway, represented by wavelet power in the 14.77-day band for chlorophyll-*a* (Chl-*a*, top panels) and nitrate (NO_3, bottom panels). The left panels correspond to the TIDES simulation, whereas the right panels show the TIDES − NOTIDES difference, thereby isolating the tidal contribution to Chl-*a* and NO_3 variability. Magenta dashed lines indicate the internal-tide pathway identified by Kouogang et al. (2025). In the Chl-*a* panels, the solid line represents the deep chlorophyll maximum (DCM) in the TIDES simulation, while the dashed line indicates the upper nitracline in the TIDES simulation. In the NO_3 panels, the blue line marks the upper nitracline in the TIDES simulation, whereas the red line corresponds to the upper nitracline in the NOTIDES simulation. The white dashed line represents the lower nitracline in the TIDES simulation, and the black dashed line represents the lower nitracline in the NOTIDES simulation.

5. Discussion

5.1 Model skill

Although the coupled physical–biogeochemical model exhibits several biases, its overall performance remains satisfactory, particularly in the offshore region, where the agreement with observations is strongest. The high spatial correlation obtained offshore for surface chlorophyll, $r = 0.9$, indicates that the model captures the main patterns of open-ocean chlorophyll variability. This provides confidence in the robustness of the simulated tidal signatures, especially along the internal-tide propagation pathway where the main mechanisms discussed in this study occur.

Model biases nevertheless remain and must be considered when interpreting the results. These biases do not question the existence of a tidal imprint on nitrate and chlorophyll distributions, but they may affect the absolute magnitude of the simulated biogeochemical response. A first source of uncertainty concerns the representation of organic matter production, transformation, and recycling, which strongly controls the relationship between nutrient supply and phytoplankton biomass. More generally, the routing of fixed carbon through the upper-ocean ecosystem and into particulate export differs substantially among marine biogeochemical models, with important consequences for particle formation and export efficiency (Laufkötter et al., 2016). In PISCES, ecosystem dynamics are represented using a limited number of plankton functional types and simplified trophic interactions (Aumont et al., 2015). Such simplifications may affect the simulated vertical chlorophyll structure, particularly the depth of the DCM, as well as the efficiency with which tidally induced nitrate redistribution is converted into phytoplankton biomass. However, they do not undermine the tidal enrichment mechanism itself. Additional uncertainty arises from the representation of river-influenced biogeochemistry, which is especially critical in the Amazon shelf system. In our configuration, dissolved organic matter, suspended matter, and sediment inputs from the Amazon River are not explicitly represented. Previous studies in the western tropical Atlantic have shown that simulated biogeochemical responses are sensitive to assumptions regarding the stoichiometry and lability of terrestrial dissolved organic matter, as well as to the partitioning between organic and inorganic nutrient inputs (Louchard et al., 2021). These factors influence where and when regenerated nutrients become available along the plume pathway, and therefore affect both nutrient distributions and biological production. Likewise, several processes that are likely important in the Amazon system remain difficult to constrain and are only partially represented in current models. These include exchanges between particulate and dissolved phosphorus, as well as the contrasting behavior of terrestrial and marine organic matter pools (Louchard et al., 2021). Such uncertainties may partly explain the remaining discrepancies between simulated and observed chlorophyll patterns, particularly over the shelf and in plume-influenced waters, aside from the intrinsic uncertainties associated with coastal ocean-color measurements (Cardoso dos Santos et al., 2025). A further limitation may arise from the atmospheric forcing. In the equatorial band, upper-ocean nitrate supply is strongly controlled by equatorial upwelling driven by trade-wind divergence, together with the depth of the nitracline, which regulates the seasonal chlorophyll response (Grodsky et al., 2008; Radenac et al., 2020). If ERA5 overestimates trade winds or near-equatorial wind divergence, it may enhance equatorial upwelling and vertical nutrient supply in the model. This could contribute to the positive nitrate bias identified in the equatorial band and, in turn, to an overestimation of chlorophyll concentrations in that region. Such behavior is consistent with a common bias of coupled physical–biogeochemical models in equatorial environments (Radenac et al., 2020).

These uncertainties highlight the need for additional sensitivity experiments to assess the influence of key biogeochemical assumptions, atmospheric forcing, and numerical choices in coupled physical–biogeochemical modelling. In particular, previous work in the Amazon region by Gévaudan et al. (2025) emphasized the importance of testing the representation of organic matter, including remineralization, optical effects, and the stoichiometry of organic and inorganic fluxes, to improve the realism of simulated chlorophyll distributions.

5.2 Coherence and incoherence of the internal tide: tide–eddy interactions

Despite these limitations, the main conclusion of this study remains robust: tides substantially modulate nitrate redistribution and chlorophyll variability over the Amazon shelf and along the internal-tide propagation pathway. The identified biases do not invalidate the dynamical–biogeochemical mechanism highlighted here, but they imply that caution is required when interpreting the absolute magnitude of the modeled response. The results should therefore be viewed as strong evidence for the existence and spatial organization of the tidal effect, while the precise amplitude of the biogeochemical response remains subject to model uncertainty.

A purely wave-like pattern could be expected from the internal-tide field. However, the model reveals a more complex spatial organization. A clear cone-shaped structure appears in the tidally related biogeochemical fields (Figure 10, top right; Figure 11, top), suggesting that the biological response to internal tides is not simply organized along a single propagation beam. This geometry is not unique to the present simulations. A similar pattern was reported by De Macedo et al. (2026), who analysed the relative chlorophyll anomaly, ΔCHL, between the day of an internal solitary wave event and the 15-day mean centred on that date for the case of 12 October 2018. Their results showed a cone-shaped chlorophyll enhancement reaching nearly 40% relative to the biweekly mean. The same feature is reproduced in Figure 14, supporting the consistency of the observed internal tide-induced biological response. The recurrence of this pattern across independent datasets suggests that it reflects a robust dynamical feature rather than a model artefact.

A closer examination indicates that the cone is composed of two distinct branches, each associated with a different physical mechanism. The first branch is aligned with the continental slope, where internal tides are generated. This interpretation is consistent with the results shown in Figure 7, where chlorophyll enrichment along the slope is driven by tidal forcing. The second branch, located farther offshore, appears to be associated with internal-tide propagation and dissipation. It coincides with the region of maximum internal-tide coherence identified in this study, which has also been described as a preferential dissipation zone by Assene et al. (2024) and Kouogang et al. (2025). In this region, Kouogang et al. (2026) showed that energy is transferred from mode-1 internal tides toward higher baroclinic modes, a process enhanced by interactions with mesoscale structures.

Further support for this interpretation comes from the spatial relationship between the conical chlorophyll signature and the surface eddy kinetic energy field. As shown in Figure 14, the edges of the chlorophyll cone are broadly aligned with the boundaries of enhanced eddy kinetic energy. This co-location suggests an active coupling between internal tides and mesoscale circulation. Because the cone is present only in the TIDES simulation (Figure 11), mesoscale activity alone

https://doi.org/10.5194/egusphere-2026-2729
Preprint. Discussion started: 27 May 2026

cannot explain its formation. Rather, the pattern is interpreted as the imprint of combined tide–eddy interactions on the chlorophyll field.

The wavelet spectra shown in Figures 11 and 12 provide a complementary view of this transition from coherent to less coherent tidal variability. At site P1, located close to the internal-tide generation region, the spectral peak is well aligned with the MSf period, as expected for a coherent spring–neap tidal modulation. Farther offshore, at site P2, the spectral peak is shifted by about 1–2 days. This offset may reflect the influence of mesoscale circulation on the propagating internal tide. Such behaviour is consistent with Tchilibou et al. (2022), who showed that internal tides can continue to propagate beyond their coherent region in an incoherent form. The offshore extension of the TIDES − NOTIDES difference in Figure 11 supports this interpretation, as it indicates that the tidal imprint persists beyond the region of maximum coherence. This persistence is also consistent with the instantaneous baroclinic energy fluxes propagating offshore, as documented by Kouogang et al. (2026).

The observed spectral shift can be interpreted through the beating mechanism between the M2 and S2 tidal constituents. Under nominal conditions, with $T_{M2} \approx 12.42\text{h}$ and $T_{S2} = 12.00\text{h}$, the beating period is

$$T_{MSf} = \frac{1}{\mid f_{S2} - f_{M2} \mid}$$

which gives the well-known fortnightly modulation of approximately 14.8 days. However, this modulation period is sensitive to small effective frequency shifts. A modest lengthening of the apparent M2 and S2 periods by about 30 minutes is sufficient to shift the beating period toward 16 days, while a lengthening of about one hour pushes it close to 17 days. Such perturbations are within the range expected from tide–eddy interactions and can therefore account for the 1–2 day offset observed between P1 and P2. This suggests that the offshore chlorophyll response reflects not only the direct spring–neap modulation of coherent internal tides, but also the distortion and partial incoherence of the tidal signal as it interacts with mesoscale variability.

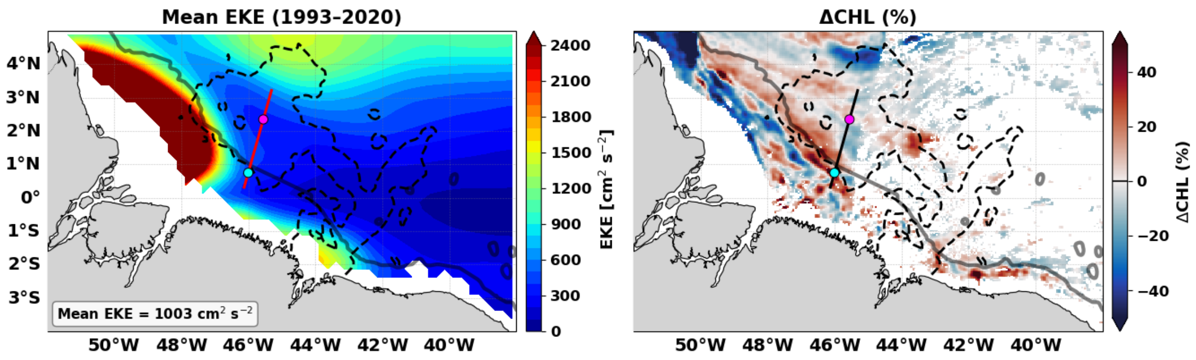

Figure 14 (a) Mean Eddy Kinetic Energy (EKE, cm² s⁻²) computed from AVISO altimetry-derived geostrophic velocities averaged over the 1993–2020 (b) Relative chlorophyll-a anomaly ΔCHL (%) on 12 October 2018,

identified as an illustrative case day of internal solitary wave (ISW). ΔCHL is computed at each pixel between the daily CHL concentration and the 15-day mean centered on the ISW day (5–19 October 2018), using Copernicus GlobColour L3 multi-sensor 4 km daily products. In both panels, the solid black line denotes the 1000 m isobath, the dashed black contour shows the 1.8 m M2 barotropic tidal amplitude derived from the MIOST altimetric product, and the colored markers (cyan, magenta) connected by a line indicate the Internal Tides pathway from the generation site (cyan) to the dissipation site (magenta)

5. Conclusion

This study used a high-resolution coupled physical–biogeochemical model at 1/36° resolution, together with twin simulations performed with and without tidal forcing over 2013–2016, to investigate how tides shape nitrate and chlorophyll-a distributions across the Amazon shelf–offshore continuum. Particular attention was given to a key region of internal-tide generation and offshore propagation, where tidal dynamics modulate biogeochemical variability from seasonal to spring–neap timescales. The model reproduces the main observed large-scale patterns of surface nitrate and chlorophyll-a, as well as the vertical nitrate structure along the internal-tide pathway, supporting its use to quantify the tidal imprint on nutrient and phytoplankton variability.

Our results show that tides exert a substantial control on the mean distribution of both nitrate and chlorophyll. At the surface, tidal effects are strongest over the northern shelf, along the shelf break, and within the main internal-tide propagation band. In these regions, tides increase surface nitrate by about 0.2–0.4 mmol NO_3 m^{-3}, locally corresponding to increases of approximately 50% or more relative to the background field. Negative nitrate anomalies of −0.2 to −0.4 mmol NO_3 m^{-3} are mainly confined to the southern shelf and nearshore regions. The chlorophyll response is more spatially heterogeneous. Tides reduce surface chlorophyll by up to about 0.2 mg Chl-a m^{-3} near the river mouth, corresponding to a decrease of roughly 30–40%, while offshore positive anomalies are generally weaker, on the order of 0.05–0.15 mg Chl-a m^{-3}. These contrasted anomalies indicate that tides not only modify nutrient availability, but also redistribute the biological response between the nearshore plume and offshore waters. Along the internal tides pathway, the vertical structure reveals a clear tidal redistribution of nitrate and chlorophyll. In the TIDES simulation, the annual-mean nitracline extends approximately from 90 to 160 m, while the deep chlorophyll maximum is centered around 25 m. Tidal forcing produces a dipolar nitrate anomaly, with nitrate decreasing by up to about 2 mmol NO_3 m^{-3} below the nitracline and increasing by a similar magnitude within the nitracline. This pattern is consistent with an upward tidal transfer of nutrients. In parallel, chlorophyll decreases within the nitracline and increases in the euphotic layer, with surface and subsurface enrichments reaching about +0.15 mg Chl-a m^{-3} near both the main internal-tide generation site and the offshore dissipation region. Together, these results indicate that tidally driven nitrate redistribution promotes chlorophyll enhancement where nutrients reach sufficiently illuminated waters. This coupling exhibits a marked seasonal modulation. Tidal effects are stronger during April–June than during August–

https://doi.org/10.5194/egusphere-2026-2729
Preprint. Discussion started: 27 May 2026

October, consistent with a shallower nitracline in April–June. During this season, the nitracline starts around 50–60 m and extends down to 130–150 m, allowing tidally uplifted nitrate to reach the lower euphotic layer more efficiently. In August–October, the nitracline is displaced downward, from about 80–100 m to approximately 150 m, reducing the efficiency of tidal nitrate supply to the illuminated layer. As a result, offshore positive chlorophyll anomalies reach about +0.10 mg Chl-a m^{-3} in April–June, compared with about +0.05 mg Chl-a m^{-3} in August–October. Along the transect, surface chlorophyll anomalies reach +0.10 to +0.15 mg Chl-a m^{-3} in April–June, compared with only +0.05 to +0.07 mg Chl-a m^{-3} in August–October. At the regional scale, the tidal contribution accounts on average for about 63% of the seasonal variability of surface nitrate, indicating that tidal forcing alone explains more than half of the seasonal nutrient signal over the study area.

Beyond the mean state and the seasonal cycle, tides generate a marked submonthly signal in the spring–neap band, with a period close to 14.77 days. In both nitrate and chlorophyll, this signal forms a coherent cone-shaped pattern extending from the shelf break into the offshore internal-tide propagation region. The chlorophyll signal is strongest near the generation site and remains detectable offshore, in agreement with satellite observations. Wavelet analyses reveal a clear spring–neap peak, together with harmonics at twice and three times the spring–neap frequency, which appear only when tides are included. This confirms the tidal origin of the submonthly biogeochemical variability.

The nitrate field exhibits a comparable spring–neap modulation, with enhanced variability near the generation site and weaker but persistent signals offshore. Vertically, chlorophyll oscillations in the spring–neap band remain mainly confined to the deep chlorophyll maximum, whereas nitrate oscillations extend over a broader depth range and reach their strongest amplitudes near the base of the nitracline. This vertical contrast suggests that phytoplankton responds to spring–neap nitrate pulsing only where tidally driven nutrient variability intersects the lower euphotic layer.

Taken together, these results demonstrate that tides are not a secondary perturbation in the Amazon shelf–offshore region, but a major driver of nitrate redistribution and chlorophyll variability from the shelf break to the offshore propagation region. Tides enhance nutrient supply within the nitracline, redistribute chlorophyll toward the euphotic layer, strengthen the seasonal nutrient cycle, and generate a strong spring–neap biogeochemical signal that extends well beyond the generation site. Although uncertainties remain in the representation of some coastal and plume-related biogeochemical processes, the main conclusion is robust: tides, and especially internal tides, are a key component of the physical–biogeochemical coupling off the Amazon shelf.

Building on these findings, future work should disentangle the relative contributions of tidal mixing and advection to the redistribution of nutrients and biomass. Extending the analysis to primary production, export production, and zooplankton biomass will be essential to better constrain the role of tidal dynamics in ecosystem functioning and carbon export in the Amazon offshore region.

Data availability

The Copernicus Marine Service global biogeochemical hindcast product GLOBAL_MULTIYEAR_BGC_001_029, distributed by Mercator Ocean International, was used to prescribe the initial and open-boundary biogeochemical conditions for PISCES. Riverine biogeochemical inputs were prescribed from the BIOMERGLORYS2V3_river.orca025deg climatological product, also provided by Mercator Ocean International. Atmospheric forcing was taken from ERA5, and Amazon River discharge was prescribed from ISBA-CTRIP monthly discharge fields adjusted using HYBAM discharge observations. Surface nitrate was evaluated against the CARS climatology. Surface chlorophyll-a was obtained from the daily Ocean Colour CCI L3 product distributed by the Copernicus Marine Service (https://doi.org/10.48670/moi-00282). Surface geostrophic currents were obtained from the delayed-time DUACS altimetry product (https://doi.org/10.48670/moi-00149). The AVISO+ products used in this study are publicly available: internal-tide sea-surface-height signatures were obtained from the MIOST-IT product (doi:10.24400/527896/a01-2022.003), and surface eddy kinetic energy was derived from the SSALTO/DUACS multi-mission altimetry monthly climatology product (doi:10.24400/527896/AVISO-2026.002). The latter is based on the CMEMS SEALEVEL_GLO_PHY_L4_REP_OBSERVATIONS_008_047 product. During the review process, the AMAZON36-BIO model outputs used in this study and the AMAZOMIX in situ observations are made available to reviewers through restricted access in the Copernicus review system. If the manuscript is accepted for publication, these datasets will be made publicly available in a FAIR-aligned repository and cited with a DOI in the reference list.

Author contributions

Funding acquisition : AKL and ACS .Conceptualization and methodology : AM , AKL, ID, VP and ACS. Model Development : FA and GM. Data processing: AM. Formal analysis: AM with interactions from all co-authors. Preparation and writing of the manuscript: AM with the contributions from all co-authors.

Competing interests

The contact author has declared that none of the authors has any competing interests.

Disclaimer

While Copernicus Publications makes every effort to include appropriate place names, the final responsibility lies with the authors. Views expressed in the text are those of the authors and do not necessarily reflect the views of the publisher."
Please feel free to add disclaimer text at your choice, if applicable.

Acknowledgements

This work is a contribution to the project "MIAMAZ-ETI" (Multi-Sensors study of the fine scale processes and their impacts on ocean color, off the Amazon shelf : Eddy-Tides Interactions). The authors thank Guillaume Morvan for providing NEMO model data. This work was performed using HPC resources from GENCI-IDRIS (Grant 2025-AD010111357R). This work was performed using HPC resources from GENCI-IDRIS (Grant 2024-AD010111357R1) (Grant 2025-AD010111357R2) (Grant 2026-AD010111357R3)

Financial support

This work is a part of the PhD thesis of Amine M'hamdi, funded by the Fundação de Amparo a Ciência e Tecnologia do Estado de Pernambuco (FACEPE) (IBPG-1078- 1.08/22), under the co-advisement of Ariane Koch-Larrouy, Alex Costa da Silva, Isabelle Dadou, and Vincent Vantrepotte. The research receive support from the "Centre National d'Études Spatiales" (CNES) through the APR MIAMAZ-728 ETI project (Principal Investigators: Ariane Koch-Larrouy, Camila Artana, Isabelle Dadou).

Review statement

The review statement will be added by Copernicus Publications listing the handling editor as well as all contributing referees according to their status anonymous or identified.

References

Aguedjou, H. M. A., Dadou, I., Chaigneau, A., Morel, Y., and Alory, G.: Eddies in the Tropical Atlantic Ocean and Their Seasonal Variability, Geophys. Res. Lett., 46, 12156–12164, https://doi.org/10.1029/2019GL083925, 2019.

Assene, F., Koch-Larrouy, A., Dadou, I., Tchilibou, M., Morvan, G., Chanut, J., Costa da Silva, A., Vantrepotte, V., Allain, D., and Tran, T.-K.: Internal tides off the Amazon shelf–Part 1: The importance of the structuring of ocean temperature during two contrasted seasons, Ocean Sci., 20, 43–67, https://doi.org/10.5194/os-20-43-2024, 2024.

Aumont, O., Éthé, C., Tagliabue, A., Bopp, L., and Gehlen, M.: PISCES-v2: an ocean biogeochemical model for carbon and ecosystem studies, Geosci. Model Dev. Discuss., 8, 1375–1509, https://doi.org/10.5194/gmd-8-2465-2015, 2015.

Baines, P. G.: On internal tide generation models, Deep Sea Res. Part Oceanogr. Res. Pap., 29, 307–338, https://doi.org/10.1016/0198-0149(82)90098-X, 1982.

Barbot, S., Lyard, F., Tchilibou, M., and Carrere, L.: Background stratification impacts on internal tide generation and abyssal propagation in the western equatorial Atlantic and the Bay of Biscay, Ocean Sci., 17, 1563–1583, https://doi.org/10.5194/os-17-1563-2021, 2021.

Beardsley, R. C., Candela, J., Limeburner, R., Geyer, W. R., Lentz, S. J., Castro, B. M., Cacchione, D., and Carneiro, N.: The M2 tide on the Amazon Shelf, J. Geophys. Res. Oceans, 100, 2283–2319, https://doi.org/10.1029/94JC01688, 1995.

Capuano, T. A., Koch-Larrouy, A., Nugroho, D., Zaron, E., Dadou, I., Tran, K., Vantrepotte, V., and Allain, D.: Impact of Internal Tides on Distributions and Variability of Chlorophyll-a and Nutrients in the Indonesian Seas, J. Geophys. Res. Oceans, 130, e2022JC019128, https://doi.org/10.1029/2022JC019128, 2025.

Cardoso dos Santos, J. F., Kampel, M., and Vantrepotte, V.: Spatiotemporal variability of chlorophyll-a concentration in the South Brazil Bight using 25 years of multi-sensor orbital data (1998–2022), Front. Remote Sens., 6, 1544375, https://doi.org/10.3389/frsen.2025.1544375, 2025.

De Macedo, C. R., Koch-Larrouy, A., Da Silva, J. C. B., Magalhães, J. M., Lentini, C. A. D., Tran, T. K., Rosa, M. C. B., and Vantrepotte, V.: Spatial and temporal variability in mode-1 and mode-2 internal solitary waves from MODIS-Terra sun glint off the Amazon shelf, Ocean Sci., 19, 1357–1374, https://doi.org/10.5194/os-19-1357-2023, 2023.

De Macedo, C. R., Koch-Larrouy, A., da Silva, J. C. B., Magalhães, J. M., Assene, F., Tran, M. D., Dadou, I., M'Hamdi, A., Tran, T. K., and Vantrepotte, V.: Tidal signatures on surface chlorophyll a concentration in the Brazilian Equatorial Margin, Ocean Sci., 22, 871–892, https://doi.org/10.5194/os-22-871-2026, 2026.

Demaster, D. J. and Pope, R. H.: Nutrient dynamics in Amazon shelf waters: results from AMASSEDS, Cont. Shelf Res., 16, 263–289, https://doi.org/10.1016/0278-4343(95)00008-O, 1996.

Didden, N. and Schott, F.: Eddies in the North Brazil Current retroflection region observed by Geosat altimetry, J. Geophys. Res. Oceans, 98, 20121–20131, https://doi.org/10.1029/93JC01184, 1993.

Egbert, G. D. and Ray, R. D.: Significant dissipation of tidal energy in the deep ocean inferred from satellite altimeter data, Nature, 405, 775–778, https://doi.org/10.1038/35015531, 2000.

Fassoni-Andrade, A. C., Durand, F., Azevedo, A., Bertin, X., Santos, L. G., Khan, J. U., Testut, L., and Moreira, D. M.: Seasonal to interannual variability of the tide in the Amazon estuary, Cont. Shelf Res., 255, 104945, https://doi.org/10.1016/j.csr.2023.104945, 2023.

Fratantoni, D. M. and Glickson, D. A.: North Brazil Current ring generation and evolution observed with SeaWiFS, J. Phys. Oceanogr., 32, 1058–1074, https://doi.org/10.1175/1520-0485(2002)032<1058:NBCRGA>2.0.CO;2, 2002.

Gabioux, M., Vinzon, S. B., and Paiva, A. M.: Tidal propagation over fluid mud layers on the Amazon shelf, Cont. Shelf Res., 25, 113–125, https://doi.org/10.1016/j.csr.2004.09.001, 2005.

Gaxiola-Castro, G., Álvarez-Borrego, S., Nájera-Martínez, S., and Zirino, A.: Internal waves effect on the Gulf of California phytoplankton, Cienc. Mar., 28, 297–309, https://doi.org/10.7773/cm.v28i3.222, 2002.

Gévaudan, M., Jouanno, J., Aumont, O., and Boutin, J.: On the Importance of Riverine Organic Matter for the Amazon Plume: A Modeling Study, J. Geophys. Res. Oceans, 130, e2024JC021527, https://doi.org/10.1029/2024JC021527, 2025.

Goes, J. I., do Rosario Gomes, H., Chekalyuk, A. M., Carpenter, E. J., Montoya, J. P., Coles, V. J., Yager, P. L., Berelson, W. M., Capone, D. G., and Foster, R. A.: Influence of the Amazon River discharge on the biogeography of phytoplankton communities in the western tropical north Atlantic, Prog. Oceanogr., 120, 29–40, https://doi.org/10.1016/j.pocean.2013.07.010, 2014.

Goret, C., Koch-Larrouy, A., Kouogang, F., de Macedo, C. R., M'Hamdi, A., Magalhães, J., da Silva, J. C. B., Tchilibou, M., Artana, C., and Dadou, I.: Internal solitary waves refraction and diffraction from interaction with eddies off the Amazon Shelf from SWOT, EGUsphere, 2025, 1–33, https://doi.org/10.5194/egusphere-2025-3933, 2025.

Grodsky, S. A., Carton, J. A., and McClain, C. R.: Variability of upwelling and chlorophyll in the equatorial Atlantic, Geophys. Res. Lett., 35, 2007GL032466, https://doi.org/10.1029/2007GL032466, 2008.

Hu, S., Townsend, D. W., Chen, C., Cowles, G., Beardsley, R. C., Ji, R., and Houghton, R. W.: Tidal pumping and nutrient fluxes on Georges Bank: a process-oriented modeling study, J. Mar. Syst., 74, 528–544, https://doi.org/10.1016/j.jmarsys.2008.04.007, 2008.

HYBAM, S.: Observation Service SO HYBAM, 2018.

Jacobsen, J. R., Edwards, C. A., Powell, B. S., Colosi, J. A., and Fiechter, J.: Nutricline adjustment by internal tidal beam generation enhances primary production in idealized numerical models, Front. Mar. Sci., 10, 1309011, https://doi.org/10.3389/fmars.2023.1309011, 2023.

Johns, W. E., Lee, T. N., Beardsley, R. C., Candela, J., Limeburner, R., and Castro, B.: Annual cycle and variability of the North Brazil Current, J. Phys. Oceanogr., 28, 103–128, https://doi.org/10.1175/1520-0485(1998)028<0103:ACAVOT>2.0.CO;2, 1998.

Kelly, S. M., Nash, J. D., and Kunze, E.: Internal-tide energy over topography, J. Geophys. Res. Oceans, 115, 2009JC005618, https://doi.org/10.1029/2009JC005618, 2010.

Kim, H., Son, Y. B., and Jo, Y.-H.: Hourly observed internal waves by geostationary ocean color imagery in the east/Japan Sea, J. Atmospheric Ocean. Technol., 35, 609–617, https://doi.org/10.1175/JTECH-D-17-0049.1, 2018.

Kossack, J., Mathis, M., Daewel, U., Zhang, Y. J., and Schrum, C.: Barotropic and baroclinic tides increase primary production on the Northwest European Shelf, Front. Mar. Sci., 10, 1206062, https://doi.org/10.3389/fmars.2023.1206062, 2023.

Kouogang, F., Koch-Larrouy, A., Magalhaes, J., Costa da Silva, A., Kerhervé, D., Bertrand, A., Cervelli, E., Assene, F., Ternon, J.-F., and Rousselot, P.: Turbulent dissipation along contrasting internal tide paths off the Amazon shelf from AMAZOMIX, Ocean Sci., 21, 1589–1608, https://doi.org/10.5194/os-21-1589-2025, 2025

Kouogang, F., Koch-Larrouy, A., Carton, X., Assene, F., Morvan, G., and Araujo, M.: Internal tides–cyclonic eddy interaction and intermodal energy pathways: evidence from 3 km NEMO-AMAZON36 simulations, Ocean Sci., 22, 1545–1568, https://doi.org/10.5194/os-22-1545-2026, 2026.

Laufkötter, C., Vogt, M., Gruber, N., Aumont, O., Bopp, L., Doney, S. C., Dunne, J. P., Hauck, J., John, J. G., and Lima, I. D.: Projected decreases in future marine export production: the role of the carbon flux through the upper ocean ecosystem, Biogeosciences, 13, 4023–4047, https://doi.org/10.5194/bg-13-4023-2016, 2016.

Lefèvre, N., Flores Montes, M., Gaspar, F. L., Rocha, C., Jiang, S., De Araújo, M. C., and Ibánhez, J. S. P.: Net heterotrophy in the Amazon continental shelf changes rapidly to a sink of CO2 in the outer Amazon plume, Front. Mar. Sci., 4, 278, https://doi.org/10.3389/fmars.2017.00278, 2017.

Louchard, D., Gruber, N., and Münnich, M.: The Impact of the Amazon on the Biological Pump and the Air-Sea CO2 Balance of the Western Tropical Atlantic, Glob. Biogeochem. Cycles, 35, e2020GB006818, https://doi.org/10.1029/2020GB006818, 2021.

Ma, L., Bai, X., Laws, E. A., Xiao, W., Guo, C., Liu, X., Chiang, K., Gao, K., and Huang, B.: Responses of Phytoplankton Communities to Internal Waves in Oligotrophic Oceans, J. Geophys. Res. Oceans, 128, e2023JC020201, https://doi.org/10.1029/2023JC020201, 2023.

Magalhaes, J. M., da Silva, J. C. B., Buijsman, M. C., and Garcia, C. A. E.: Effect of the North Equatorial Counter Current on the generation and propagation of internal solitary waves off the Amazon shelf (SAR observations), Ocean Sci., 12, 243–255, https://doi.org/10.5194/os-12-243-2016, 2016.

Mahadevan, A.: The Impact of Submesoscale Physics on Primary Productivity of Plankton, Annu. Rev. Mar. Sci., 8, 161–184, https://doi.org/10.1146/annurev-marine-010814-015912, 2016.

M'hamdi, A., Koch-Larrouy, A., Costa da Silva, A., Dadou, I., De Macedo, C. R., Bosse, A., Vantrepotte, V., Aguedjou, H. M., Tran, T.-K., and Testor, P.: Impact of internal tides on chlorophyll a distribution and primary production off the Amazon shelf from glider measurements and satellite observations, Ocean Sci., 21, 2873–2894, https://doi.org/10.5194/os-21-2873-2025, 2025.

Molleri, G. S. F., Kampel, M., and de Moraes Novo, E. M. L.: Spectral classification of water masses under the influence of the Amazon River plume, Acta Oceanol. Sin., 29, 1–8, https://doi.org/10.1007/s13131-010-0031-1, 2010.

Muacho, S., da Silva, J. C. B., Brotas, V., Oliveira, P. B., and Magalhaes, J. M.: Chlorophyll enhancement in the central region of the Bay of Biscay as a result of internal tidal wave interaction, J. Mar. Syst., 136, 22–30, https://doi.org/10.1016/j.jmarsys.2014.03.016, 2014.

Muller-Karger, F. E., McClain, C. R., and Richardson, P. L.: The dispersal of the Amazon's water, Nature, 333, 56–59, https://doi.org/10.1038/333056a0, 1988.

Müller-Karger, F. E., McClain, C. R., Fisher, T. R., Esaias, W. E., and Varela, R.: Pigment distribution in the Caribbean Sea: Observations from space, Prog. Oceanogr., 23, 23–64, https://doi.org/10.1016/0079-6611(89)90024-4, 1989.

Munk, W. and Wunsch, C.: Abyssal recipes II: energetics of tidal and wind mixing, Deep Sea Res. Part Oceanogr. Res. Pap., 45, 1977–2010, https://doi.org/10.1016/S0967-0637(98)00070-3, 1998.

Olivier, L., Boutin, J., Reverdin, G., Lefèvre, N., Landschützer, P., Speich, S., Karstensen, J., Labaste, M., Noisel, C., and Ritschel, M.: Wintertime process study of the North Brazil Current rings reveals the region as a larger sink for CO2 than expected, Biogeosciences, 19, 2969–2988, https://doi.org/10.5194/bg-19-2969-2022, 2022.

Olivier, L., Reverdin, G., Boutin, J., Laxenaire, R., Iudicone, D., Pesant, S., Calil, P. H., Horstmann, J., Couet, D., and Erta, J. M.: Late summer northwestward Amazon plume pathway under the action of the North Brazil Current rings, Remote Sens. Environ., 307, 114165, https://doi.org/10.1016/j.rse.2024.114165, 2024.

Prestes, Y. O., da Silva, A. C., and Jeandel, C.: Amazon water lenses and the influence of the North Brazil Current on the continental shelf, Cont. Shelf Res., 160, 36–48, https://doi.org/10.1016/j.csr.2018.04.002, 2018.

Radenac, M.-H., Jouanno, J., Tchamabi, C. C., Awo, M., Bourlès, B., Arnault, S., and Aumont, O.: Physical drivers of the nitrate seasonal variability in the Atlantic cold tongue, Biogeosciences, 17, 529–545, https://doi.org/10.5194/bg-17-529-2020, 2020.

Ray, R. D. and Susanto, R. D.: Tidal mixing signatures in the Indonesian seas from high-resolution sea surface temperature data, Geophys. Res. Lett., 43, 8115–8123, https://doi.org/10.1002/2016GL069485, 2016.

Richardson, P. L., Hufford, G. E., Limeburner, R., and Brown, W. S.: North Brazil Current retroflection eddies, J. Geophys. Res. Oceans, 99, 5081–5093, https://doi.org/10.1029/93JC03486, 1994.

Ridgway, K. R., Dunn, J. R., and Wilkin, J. L.: Ocean interpolation by four-dimensional weighted least squares—Application to the waters around Australasia, J. Atmospheric Ocean. Technol., 19, 1357–1375, https://doi.org/10.1175/1520-0426(2002)019<1357:OIBFDW>2.0.CO;2, 2002.

Ruault, V., Jouanno, J., Durand, F., Chanut, J., and Benshila, R.: Role of the Tide on the Structure of the Amazon Plume: A Numerical Modeling Approach, J. Geophys. Res. Oceans, 125, e2019JC015495, https://doi.org/10.1029/2019JC015495, 2020.

Sharples, J., Tweddle, J. F., Mattias Green, J. A., Palmer, M. R., Kim, Y.-N., Hickman, A. E., Holligan, P. M., Moore, C. M., Rippeth, T. P., Simpson, J. H., and Krivtsov, V.: Spring-neap modulation of internal tide mixing and vertical nitrate fluxes at a shelf edge in summer, Limnol. Oceanogr., 52, 1735–1747, https://doi.org/10.4319/lo.2007.52.5.1735, 2007.

Silva, A., Araujo, M., Medeiros, C., Silva, M., and Bourles, B.: Seasonal changes in the mixed and barrier layers in the western equatorial Atlantic, Braz. J. Oceanogr., 53, 83–98, https://doi.org/10.1590/S1679-87592005000200001, 2005.

Silva, A. C., Bourlès, B., and Araujo, M.: Circulation of the thermocline salinity maximum waters off the Northern Brazil as inferred from in situ measurements and numerical results, in: Annales Geophysicae, 1861–1873, https://doi.org/10.5194/angeo-27-1861-2009, 2009.

Smith Jr, W. O. and Demaster, D. J.: Phytoplankton biomass and productivity in the Amazon River plume: correlation with seasonal river discharge, Cont. Shelf Res., 16, 291–319, https://doi.org/10.1016/0278-4343(95)00007-N, 1996.

Subirade, C., L'hégaret, P., Speich, S., Laxenaire, R., Karstensen, J., and Carton, X.: Combining an eddy detection algorithm with in-situ measurements to study north brazil current rings, Remote Sens., 15, 1897, https://doi.org/10.3390/rs15071897, 2023.

Subramaniam, A., Yager, P. L., Carpenter, E. J., Mahaffey, C., Björkman, K., Cooley, S., Kustka, A. B., Montoya, J. P., Sañudo-Wilhelmy, S. A., Shipe, R., and Capone, D. G.: Amazon River enhances diazotrophy and carbon sequestration in the tropical North Atlantic Ocean, Proc. Natl. Acad. Sci., 105, 10460–10465, https://doi.org/10.1073/pnas.0710279105, 2008.

Tchilibou, M., Koch-Larrouy, A., Barbot, S., Lyard, F., Morel, Y., Jouanno, J., and Morrow, R.: Internal tides off the Amazon shelf during two contrasted seasons: interactions with background circulation and SSH imprints, Ocean Sci., 18, 1591–1618, https://doi.org/10.5194/os-18-1591-2022, 2022.

Torrence, C. and Compo, G. P.: A practical guide to wavelet analysis, Bull. Am. Meteorol. Soc., 79, 61–78, https://doi.org/10.1175/1520-0477(1998)079<0061:APGTWA>2.0.CO;2, 1998.

Tuerena, R. E., Williams, R. G., Mahaffey, C., Vic, C., Green, J. A. M., Naveira-Garabato, A., Forryan, A., and Sharples, J.: Internal Tides Drive Nutrient Fluxes Into the Deep Chlorophyll Maximum Over Mid-ocean Ridges, Glob. Biogeochem. Cycles, 33, 995–1009, https://doi.org/10.1029/2019GB006214, 2019.

Xing, Q., Yu, H., Yu, H., Wang, H, Ito, S., and Yuan, C.: Evaluating the spring-neap tidal effects on chlorophyll-a variations based on the geostationary satellite, Front. Mar. Sci., 8, 758538, https://doi.org/10.3389/fmars.2021.758538, 2021.

1090

Zaron, E. D., Capuano, T. A., and Koch-Larrouy, A.: Fortnightly variability of Chl a in the Indonesian seas, Ocean Sci., 19, 43–55, https://doi.org/10.5194/os-19-43-2023, 2023.